Functional characterization and lineage analysis of broadly neutralizing human antibodies against dengue virus identified by single B cell transcriptomics

Natasha D. Durham[1*^], Aditi Agrawal[1*], Eric Waltari[1], Derek Croote[2], Fabio Zanini[2+], Edgar Davidson[3], Mallorie Fouch[3], Olivia Smith[1], Esteban Carabajal[1], John E. Pak[1], Benjamin J. Doranz[3], Makeda Robinson[4,5], Ana M. Sanz[6], Ludwig L. Albornoz[7], Fernando Rosso[6,8], Shirit Einav[4,5], Stephen R. Quake[1,2], Krista M. McCutcheon[1], Leslie Goo[1,9#].

[1]Chan Zuckerberg Biohub, San Francisco, United States
[2]Department of Bioengineering, Stanford University, Stanford, United States
[3]Integral Molecular, Inc., Philadelphia, United States
[4]Division of Infectious Diseases and Geographic Medicine, Department of Medicine, Stanford University School of Medicine, Stanford, United States
[5]Department of Microbiology and Immunology, Stanford University School of Medicine, Stanford, United States
[6]Clinical Research Center, Fundación Valle del Lili, Cali, Colombia
[7]Pathology and Laboratory Department, Fundación Valle del Lili, Cali, Colombia.
[8]Department of Internal Medicine, Division of Infectious Diseases, Fundación Valle del Lili, Cali, Colombia
[9]Fred Hutchinson Cancer Research Center, Seattle, United States

[*]Equal contribution
[^]Current affiliation: Department of Microbiology and Physiological Systems, University of Massachusetts Medical School, Worcester, United States
[+]Current affiliation: Lowy Cancer Research Center, University of New South Wales, Kensington, NSW, Australia
[#]Corresponding author: lgoo@fredhutch.org

Abstract

Eliciting broadly neutralizing antibodies (bNAbs) against the four dengue virus serotypes (DENV1-4) that are spreading into new territories is an important goal of vaccine design. To delineate bNAb targets, we characterized 28 monoclonal antibodies belonging to expanded and hypermutated clonal families identified by transcriptomic analysis of single plasmablasts from DENV-infected individuals. Among these, we identified two somatically related bNAbs that potently neutralized DENV1-4. Mutagenesis studies revealed that the major recognition determinants of these bNAbs are in E protein domain I, distinct from the only known class of human bNAbs against flaviviruses with a well-defined epitope. B cell repertoire analysis from acute-phase peripheral blood suggested a memory origin and divergent somatic hypermutation pathways for these bNAbs, and a limited number of mutations was sufficient for neutralizing activity. Our study suggests multiple B cell evolutionary pathways leading to DENV bNAbs targeting a novel epitope that can be exploited for vaccine design.

Introduction

Dengue virus (DENV) is an enveloped, positive-stranded RNA virus belonging to the *Flavivirus* genus, which includes clinically significant human pathogens such as Yellow Fever virus (YFV), Japanese encephalitis virus (JEV), West Nile virus (WNV), and Zika virus (ZIKV). DENV is transmitted to humans via *Aedes* mosquitoes, whose global distribution places half of the world's population at risk for infection (Kraemer et al., 2019; Messina et al., 2019). Each year, the four phylogenetically and antigenically distinct DENV serotypes (DENV1-4) cause approximately 400 million infections (Bhatt et al., 2013). Additionally, increased global trade, connectivity, and climate change have fueled the expansion of DENV1-4 into new territories (Kraemer et al., 2019; Messina et al., 2014).

Approximately 20% of DENV-infected individuals develop a mild febrile illness, of which 5% to 20% progress to potentially fatal severe disease, characterized by bleeding, plasma leakage, shock, and organ failure (Guzman & Harris, 2015; Khursheed et al., 2013; Thein, Leo, Lee, Sun, & Lye, 2011). Epidemiological studies have shown that pre-existing antibodies from a primary DENV infection are a risk factor for severe disease following subsequent infection with a heterologous DENV serotype (Katzelnick et al., 2017; Salje et al., 2018; Sangkawibha et al., 1984). This is partly attributed to the prevalence of cross-reactive antibodies from the initial infection that can bind, but not neutralize the secondary heterologous virus. Instead, these non-neutralizing antibodies have the potential to facilitate viral uptake into Fc gamma receptor-expressing target cells in a process known as antibody-dependent enhancement (ADE) (Guzman & Harris, 2015; Halstead, 2014). Recent studies of clinical cohorts demonstrated that the risk of severe disease following secondary infection is greatest when pre-existing titers of cross-reactive antibodies fall within a narrow, intermediate range (Katzelnick et al., 2017; Salje et al., 2018). To limit the potential for ADE, an effective vaccine must therefore elicit durable and potent neutralizing antibodies of high titer against DENV1-4 simultaneously. However, the viral and host determinants leading to such bNAbs against flaviviruses are poorly understood.

All of the leading DENV vaccine candidates in clinical development are based on a tetravalent strategy (Scherwitzl, Mongkolsapaja, & Screaton, 2017), which assumes that the use of representative viral strains from each serotype will elicit a balanced and potent polyclonal antibody response to minimize the risk of ADE. However, the suboptimal efficacy and safety profile of a recently licensed DENV vaccine has been partly attributed to its inability to generate a balanced neutralizing antibody response to all four serotypes (Hadinegoro et al., 2015). Additionally, there may be important antigenic differences between circulating and lab-adapted strains (Lim et al., 2019; Raut et al., 2019), as well as among strains even within a given serotype (Bell, Katzelnick, & Bedford, 2019; Katzelnick et al., 2015). Antigenic mismatch between vaccine and circulating strains impacted vaccine efficacy (Juraska et al., 2018), highlighting the importance of rational selection of vaccine components. An alternative strategy, largely exemplified by vaccine development efforts for HIV (Kwong & Mascola, 2018) and respiratory syncytial virus (RSV) (Crank et al., 2019), relies on identifying antibodies with desirable properties and precisely defining their epitopes to guide epitope-based vaccine design (Graham, Gilman, & McLellan, 2019). For antigenically diverse viruses such as DENV, a

conserved epitope-based vaccine strategy to elicit a broad and potent monoclonal neutralizing antibody response could mitigate the challenge of selecting representative vaccine strains.

The main target of flavivirus neutralizing antibodies is the envelope (E) glycoprotein, which consists of three structural domains (DI, DII, DIII), and is anchored to the viral membrane via a helical stem and transmembrane domain. The E proteins direct many steps of the flavivirus life cycle, including entry, fusion, and assembly of new virus particles (Pierson & Diamond, 2012). Flaviviruses bud into the endoplasmic reticulum lumen as immature particles with a spiky surface on which E proteins associate into sixty heterotrimers with a chaperone protein, prM (Prasad et al., 2017; Y. Zhang et al., 2003; Y. Zhang, Kaufmann, Chipman, Kuhn, & Rossmann, 2007). Within the low pH environment of the trans-golgi network, E proteins undergo conformational changes that allow furin-mediated cleavage of prM (Yu et al., 2008), resulting in the release of mature infectious virions with a smooth surface densely coated with ninety E homodimers (Kostyuchenko et al., 2016; Kuhn et al., 2002; Mukhopadhyay, Kim, Chipman, Rossmann, & Kuhn, 2003; Sirohi et al., 2016; X. Zhang et al., 2013). The dense arrangement of E proteins on the virion surface is important for antigenicity, as many potently neutralizing human antibodies against flaviviruses target quaternary epitopes spanning multiple E proteins (de Alwis et al., 2012; Hasan et al., 2017; Kaufmann et al., 2010; Rouvinski et al., 2015; Teoh et al., 2012).

Recent advances in monoclonal antibody isolation and characterization (Boonyaratanakornkit & Taylor, 2019; Corti & Lanzavecchia, 2014) have accelerated the identification of bNAbs, including those against flaviviruses. Examples include antibodies d488 (Li et al., 2019) and m366 (Hu et al., 2019), which were cloned from B cells of rhesus macaques receiving an experimental DENV vaccine and from healthy flavivirus-naive humans, respectively, and mAb DM25-3, which was isolated from a mouse immunized with a mature form of DENV2 virus-like particles ((Shen et al., 2018). Although these antibodies are cross-reactive against DENV1-4, they demonstrated only moderate potency. E protein residues involved in d488 binding lie at the interface of the M protein and the E protein ectodomain (Li et al., 2019), while those for m366.6 binding appear to be located at the dimerization interface between DII and DIII (Hu et al., 2019). Residue W101 within the DII fusion loop was identified to be important for recognition by mAb DM25-3 (Shen et al., 2018). Attempts to engineer mouse antibodies with increased breadth and potency against DENV1-4 have also been described (Deng et al., 2011; Shi et al., 2016; Tharakaraman et al., 2013).

Only a few naturally occurring human bNAbs against flaviviruses have been characterized. Many of these antibodies target epitopes consisting of the DII fusion loop as well as the adjacent bc loop in DII in some cases (Smith et al., 2013; Tsai et al., 2013; Xu et al., 2017). Although antibodies recognizing the highly conserved fusion loop can demonstrate broad reactivity to all DENV serotypes and related flaviviruses, their neutralizing potency is often limited due to this epitope being largely inaccessible, especially on mature virions (Cherrier et al., 2009; Nelson et al., 2008; Shen et al., 2018; Stiasny, Kiermayr, Holzmann, & Heinz, 2006). To date, the most well-characterized class of human antibodies with broad and potent neutralizing activity against flaviviruses targets a conserved, quaternary epitope spanning both

E monomeric subunits within the dimer. A subset of these E dimer epitope (EDE)-specific bNAbs potently neutralize not only DENV1-4, but also ZIKV, owing to the high conservation of the EDE, which overlaps the prM binding site on E (Barba-Spaeth et al., 2016; Dejnirattisai et al., 2015; Rouvinski et al., 2015). The exciting discovery of the EDE class of bNAbs highlights the potential for an epitope-focused flavivirus vaccine strategy.

As multiple specificities are likely required to provide maximum coverage of diverse circulating viral variants (Bell et al., 2019; Doria-Rose et al., 2012; Goo, Jalalian-Lechak, Richardson, & Overbaugh, 2012; Katzelnick et al., 2015; Keeffe et al., 2018; Kong et al., 2015), in this study, we aimed to define novel sites on the flavivirus E protein that can be targeted by bNAbs. By characterizing 28 monoclonal antibodies from the plasmablasts of two DENV-infected individuals, we identified J8 and J9, clonally related bNAbs that neutralized DENV1-4 in the low picomolar range. The major recognition determinants for J8 and J9 were in E protein DI, distinct from previously characterized bNAbs. Analysis of the corresponding B cell repertoire revealed divergent evolution of J8 and J9, suggesting multiple evolutionary pathways to generate bNAbs within this lineage. Our work identifies both viral and host determinants of the development of DENV bNAbs that can guide immunogen design and evaluation.

Results

Identification of cross-reactive neutralizing antibodies from clonally expanded plasmablasts of DENV-infected individuals

We previously profiled the single-cell transcriptomics of peripheral blood mononuclear cells (PBMCs) from six dengue patients and four healthy individuals (Zanini et al., 2018). In two DENV-infected patients (013 and 020), we identified 15 clonal families comprising a total of 38 unique paired heavy (VH) and light (VL) chain IgG1 plasmablast sequences, some of which were hypermutated (1.67% to 10.77% for VH, 0.67% to 7.22% for VL; Figure S1). One clonal family (CF) included members found in both individuals (antibodies B10, M1, and D8 from CF1, Figure S1), suggesting convergent evolution, which has been described for the antibody response to distinct viruses, including flaviviruses (Parameswaran et al., 2013; Robbiani et al., 2017), Ebola virus (Davis et al., 2019) and HIV (Scheid et al., 2011; Wu et al., 2011). To functionally characterize these monoclonal antibodies (mAbs), we successfully cloned 36 paired VH and VL sequences into expression vectors, and transfected mammalian cells for small scale (96-well) recombinant IgG1 production. We detected secreted IgG in the transfection supernatants for 28 of 36 mAbs, which were tested for binding to DENV2 recombinant soluble E protein (rE) and reporter virus particles (RVPs), as well as for neutralizing activity against a panel of flavivirus RVPs, including DENV1-4, ZIKV, and WNV (Figure S1). Seventeen of 28 mAbs bound to either DENV2 rE (n = 1), or RVPs (n = 7), or both (n = 9). None of the mAbs neutralized ZIKV, but all 28 neutralized at least one DENV serotype, 21 mAbs neutralized two or more DENV serotypes, and one mAb neutralized WNV in addition to DENV.

Binding profile of mAbs

For further characterization, we selected six mAbs for larger scale production and IgG purification based on their ability to neutralize at least four of the six RVPs tested. These

included two mAb clonal variants found in both patients (B10 from patient 020 and M1 from patient 013), two (C4, J9) and one (L8) patient 013 and patient 020 mAbs, respectively, that neutralized DENV1-4, and the only mAb that neutralized WNV (I7 from patient 020). We first confirmed binding activity at a single antibody concentration (5 µg/ml) by ELISA. Consistent with our pilot screen using crude IgG-containing supernatant (Figure S1), I7, M1, B10, and L8 bound to both rE and RVPs, while C4 and J9 bound to RVPs only (Figure 1A & B), suggesting that these mAbs target epitopes preferentially displayed on the intact virion. As incubation at higher temperatures has been shown to improve exposure of some epitopes (Dowd, Jost, Durbin, Whitehead, & Pierson, 2011; Lok et al., 2008; Sukupolvi-Petty et al., 2013), we performed the ELISA at both ambient temperature and 37°C. For most antibodies, incubation at 37°C resulted in a modest but consistent increase in RVP binding (Figure 1B). To evaluate the relative binding of the mAbs to rE and RVP, we also performed a dose-responsive indirect ELISA at ambient temperature (Figure 1C). Binding curves revealed robust binding of mAbs L8, B10, M1, and I7 to DENV2 rE (EC50 range of 0.4 to 23 ng/ml) while J9, C4 and the EDE mAbs C10 and B7 displayed little to no binding to rE even at high antibody concentrations (up to 200 µg/mL). All mAbs showed binding to DENV2 RVP to varying extents, with relatively high EC50 values for J9 (200 ng/ml), J8 (213 ng/ml), and C4 (1200 ng/ml), suggesting limited affinity maturation (Figure 1D).

Neutralization potency of mAbs

We next performed dose-response neutralization assays to obtain IC_{50} values (mAb concentration at which 50% of virus infectivity was inhibited). Antibodies M1, B10, and L8 displayed modest (average IC_{50} range of 379 to 796 ng/ml) and incomplete neutralization of DENV1-4, with ~10% to ~50% infectivity persisting at the highest mAb concentration tested (10 µg/ml) (Figures 2A-B). Incomplete neutralization is commonly observed for cross-reactive DII fusion loop-specific antibodies, and likely represents structurally heterogeneous virions on which the epitope is not displayed frequently enough for antibodies to bind at a stoichiometry sufficient for neutralization (Nelson et al., 2008; Pierson et al., 2007). Antibody I7 displayed an unusual neutralization profile as it did not neutralize DENV4, and its potency against DENV1-3 was lower than that against the more antigenically distant WNV. Although mAb C4 completely neutralized DENV1-4, it did so with modest potency, especially against DENV4 (IC_{50} > 1000 ng/ml). The most potent mAb we identified was J9, which despite relatively weak binding (Figure 1), completely neutralized DENV1-4 with average IC_{50} values of 6 ng/ml, 30 ng/ml, 15 ng/ml, and 39 ng/ml, respectively. A previously characterized subgroup of the EDE class of bNAbs, which includes mAb EDE1 C10 can neutralize not only DENV1-4, but also ZIKV (Barba-Spaeth et al., 2016). J9 showed a high specificity for DENV, with no activity against ZIKV, and up to ~60-fold greater potency against some DENV serotypes compared to EDE1 C10 (Figure 2B). Depending on the serotype, the average neutralization potency of J9 against DENV1-4 was also up to 15-fold higher than that of bNAb EDE2 B7, which belongs to another EDE subgroup with poor neutralizing activity against ZIKV (Barba-Spaeth et al., 2016).

The broad and potent neutralizing activity of J9 prompted us to re-evaluate our pilot results obtained for J8, a somatic variant with no binding or neutralizing activity in our screen with crude IgG-containing supernatant (Figure S1). When we repeated the cloning, expression, and

purification of J8 IgG, we observed similar binding (Figure 1) and neutralization (Figure 2) profiles to J9. When tested as Fab fragments, J9 and J8 were still able to potently neutralize DENV, unlike C4 and EDE1 C10, which failed to achieve 50% neutralization at the highest mAb concentration tested (Figure S2). J9 and J8 also potently neutralized contemporary DENV1-4 isolates with IC_{50} values < 50 ng/ml (Figure S3). Additionally, in contrast to C4 and the cross-reactive DII fusion loop-specific mouse mAb E60 (Goo, VanBlargan, Dowd, Diamond, & Pierson, 2017; Nelson et al., 2008; Oliphant et al., 2006), but similar to EDE bNAbs (Dejnirattisai et al., 2015), J9 and J8 potently neutralized DENV regardless of virion maturation state (Figure S4), which can indirectly modulate epitope exposure (Cherrier et al., 2009; Goo et al., 2019; Nelson et al., 2008) and has been shown to be distinct among circulating versus lab-adapted strains (Raut et al., 2019). We also tested the ability of mAbs to mediate neutralization after virus attachment to cells, which is characteristic of many potently neutralizing antibodies against flaviviruses (Goo et al., 2019; Nybakken et al., 2005; Sukupolvi-Petty et al., 2010; Vogt et al., 2009; Xu et al., 2017). When added after virus attachment to Raji-DCSIGNR cells, C4 failed to inhibit 40-50% of infection at the highest mAb concentration tested (300 µg/ml) (Figure 3). In contrast, J9, J8, and EDE1 C10 potently inhibited DENV2 infection both pre- and post-virus attachment to cells.

ADE potential of mAbs

In vitro, antibodies can mediate ADE of infection in cells expressing Fc gamma receptor (FcγR) at sub-neutralizing concentrations (Pierson et al., 2007). Recent studies in humans have also demonstrated that the risk of severe dengue disease following secondary infection is greatest within a range of intermediate titers of pre-existing DENV-specific antibodies, while higher titers are protective against symptomatic infection (Katzelnick et al., 2017; Salje et al., 2018). Thus, eliciting potently neutralizing antibodies is desirable to limit the concentration range within which ADE can occur. We measured the ADE potential of a subset of the mAbs identified above in K562 cells, which have been used extensively to study ADE of flaviviruses as they express FcγR and are poorly permissive for infection in the absence of antibody (Littaua, Kurane, & Ennis, 1990). As expected, all DENV-specific mAbs mediated ADE of DENV2 infection to varying extents (Figure S5). We measured the antibody concentration at which the highest level of ADE was observed (peak enhancement titer). Consistent with their high neutralization potencies, the average peak enhancement titer of J9 and J8 for DENV2 (3 ng/ml) was approximately 27-fold and 480-fold lower than that of mAbs EDE1 C10 (80 ng/ml) and C4 (1467 ng/ml), respectively (Figures S5A and S5D). For J9, J8, and EDE bNAbs, DENV2 neutralization occurred beyond the peak enhancement titer, with no infectivity observed at high antibody concentrations. In contrast, for C4 and L8, which neutralized DENV relatively weakly (Figure 1), ADE of DENV2 was still detected at the highest concentration (10 µg/ml) tested (Figure S5A). Even at high concentrations, L8 also mediated ADE of ZIKV (Figure S5B) and WNV (Figure S5C), suggesting binding, but not neutralizing activity against these viruses (Figure 1). Consistent with their ability to recognize ZIKV, EDE bNAbs enhanced ZIKV infection at sub-neutralizing concentrations (Figure S5B). J9 and J8 did not facilitate ADE of ZIKV nor WNV infection, suggesting lack of binding to these flaviviruses. Given their high neutralization potencies against DENV1-4, J9 and J8 represent desirable antibodies to elicit as their ADE

potential is restricted to a narrow range of low antibody concentrations, beyond which neutralization is observed.

Epitope specificity of mAbs

To identify amino acid residues required for mAb recognition, we screened a shotgun alanine-scanning mutagenesis library of DENV2 E protein variants for mAb binding by flow cytometry (Davidson & Doranz, 2014). MAb binding profiles to this entire library are summarized in Table S1. MAbs M1 and L8 demonstrated loss of binding to variants encoding W101A and F108A mutations within the DII fusion loop (Figure 4A). Similar to a subset of previously described fusion loop-specific antibodies (Cherrier et al., 2009; Smith et al., 2013; Tsai et al., 2013), M1 recognition also depended on residue G106 within the fusion loop and residue 75 on the adjacent bc loop (Figure 4A). Specificity for the fusion loop epitope likely contributes to the inability of these mAbs to neutralize completely, even at high concentrations (Figures 2A-B), as previously described (Dowd et al., 2011; Nelson et al., 2008). The I7 epitope involved DII residues Q256 and G266 (Figure 4B), which are conserved among many flaviviruses (indicated by yellow squares in Figure S6A alignment) and are important for recognition by the recently described cross-reactive mAb (d448) isolated from vaccinated rhesus macaques (Li et al., 2019). Unlike I7, d448 neutralized DENV4, but not WNV (Li et al., 2019). Despite testing different temperature and pH conditions, we did not detect C4 binding to WT DENV2 in this flow cytometry-based assay (data not shown) and were thus unable to screen against the mutant library. For J9, most E protein mutations that reduced binding by >80% relative to WT (shown in bold in Table S1) were found in DI (R2, I4, K47, S145, H149, N153, T155), but G102 within DII fusion loop and DII N242, as well as DIII N366 were also important (Figure 4C). These mutations minimally affected EDE1 C10 binding (Figure 4C).

For further epitope mapping of J9, one of the most potent bNAbs we identified, we first attempted to select for neutralization escape viral variants but were unsuccessful after six serial passages in cell culture under mAb selection pressure. We noted that J9 neutralized DENV1-4 but not ZIKV (Figure 1). As an alternative epitope mapping approach, we generated a panel of DENV2 RVP variants encoding individual mutations at solvent accessible E protein residues on the mature DENV virion that are identical or chemically conserved across representative DENV1-4 strains but differ from ZIKV (Figure S6A). These residues in DENV2 16681 E were substituted for analogous residues in ZIKV H/PF/2013. We also included a subset of alanine mutants identified by our binding screen to confirm their importance for neutralization. In total, we generated 34 DENV2 RVP variants encoding individual mutations throughout the E protein (Figure S6B); 31 of these variants retained sufficient infectivity (Figure S7) for neutralization studies. Most individual mutations displayed minimal (< 2-fold) effects on J9 neutralization potency (Figure S8A). Two DI mutations, K47T and V151T resulted in a modest 4-fold increase in IC_{50} (Figure S8A). Consistent with our binding screen, we confirmed that mutation at residue N153 or T155, each of which results in a loss of a potential N-linked glycosylation site, abrogated J9 neutralization, while mutation at N242 resulted in a 5-fold reduction in potency (Figures S8A). Although our binding screen suggested that individual G102A and S145A mutations contributed to J9 recognition, they had limited effects (~2-fold) on neutralization potency (Figure S8A).

Because we observed only modest effects with single mutations, we next generated DENV2 RVPs encoding the K47T and V151T mutations in combination, as well as 8 additional pairs of mutations at a subset of the above 34 residues selected based on their proximity to each other on the E dimer structure (Figure S6C). Seven of 8 DENV2 RVP variants encoding paired mutations retained infectivity (Figure S7). Five combinations of paired mutations displayed similarly modest (up to 4-fold) effects on J9 neutralization potency as when these mutations were tested individually (Figure S8A). However, in combination, K47T+V151T reduced J9 potency by almost 100-fold. In combination with the F279S mutation in DI, K47T also resulted in a 16-fold average reduction in J9 potency (Figure S8A). Figures 5A-B highlight key residues that reduced J9 neutralization potency, either alone or in combination, as identified from our screen against the entire panel of single and double mutants (Figure S8).

As seen for J9, individual mutations at residues N153 and N155, which together encode a potential N-linked glycosylation site, abrogated the neutralizing activity of the somatically related bNAb, J8 (Figure 5C). To varying extents, a similar set of individual and paired mutations that reduced J9 neutralization potency, including V151T, N242A, K47T+V151T, and H149S+V151T, also reduced J8 and C4 neutralization potency (Figures 5C-D). However, individual mutations at some DII and DIII residues that did not impact J9 neutralization potency (Figure S8A) did modestly increase resistance to neutralization by J8 (Figure S8B) and C4 (Figure S8C), respectively by 4- to 7-fold. Interestingly, the V151T mutation alone or in combination with either K47T or H149S increased neutralization potency of EDE1 C10 by 25-fold (Figure 5E). These mutations had minimal (< 2-fold) effects on the neutralizing activity of EDE2 B7 (Figure 5F) as well as patient 013 polyclonal serum (Figure S9), suggesting that they did not globally alter antigenicity. As previously shown (Dejnirattisai et al., 2015; Rouvinski et al., 2015), mutation at residue N153 or N155 improved and disrupted EDE1 C10 and EDE2 B7 recognition, respectively (Figures 5E-F). Overall, these results suggest that the recognition determinants of J9, J8, and C4, are distinct from those targeted by EDE-specific and other previously characterized bNAbs against DENV1-4 (Dejnirattisai et al., 2015; Hu et al., 2019; Li et al., 2019; Smith et al., 2013; Tsai et al., 2013; Xu et al., 2017).

Lineage analysis reveals memory origin and divergent evolution of bNAbs

To gain insight into the development of bNAbs J9 and J8, we processed PBMCs of patient 013 (from which these bNAbs were identified) obtained four days post-fever onset, and performed next generation sequencing (NGS) of the B cell receptor (BCR) repertoire. This patient experienced acute secondary infection with DENV4 (Zanini et al., 2018). Given its greater junctional diversity compared to light chain, we focused our analysis on the heavy chain repertoire, which is sufficient to identify clonal relationships (Zhou & Kleinstein, 2019). We have recently shown that PBMC stimulation in a polyclonal, BCR-independent manner can selectively expand antigen-specific memory B cells (Waltari, McGeever, Friedland, Kim, & McCutcheon, 2019). Accordingly, we obtained 8-fold more unique VH sequences from stimulated PBMCs with a greater representation of IgG over IgM clonal families compared to unstimulated PBMCs (Table S2). Compared to previously described healthy BCR repertoire data (Waltari et al., 2019), VH1-69, VH3-30, VH3-30-3, VH4-34, VH4-39 and VH4-59 were the most dominant

across both unstimulated and stimulated PBMC VH families in patient 013 (average >= 5% of repertoire; Figure S10).

We found 579 and 43,179 VH sequences related to J9/J8 in unstimulated and stimulated PBMCs, respectively (0.4% and 3.5% of total reads, respectively, Table S3). For lineage construction (Figure 6A), we included sequences that met one of three criteria: 1) highest numbers of unique molecular identifier (UMI) counts (>35 in PBMC repertoire and >150 in stimulated PBMC repertoire IgG sequences and >15 in IgA sequences), 2) < 5% somatic hypermutation, or 3) 97% identity to J9 or J8. The J9/J8 lineage derived from recombination of IGHV1-69 with IGHD2-2 and IGHJ5 with no CDRH3 insertions or deletions (Figure 6B). The majority of the clonal family members were of the IgG_1 subtype, with no IgM identified having a UMI count >2 and only a small percentage of IgA (1.8% of stimulated PBMC relatives; Figure 6A, triangles).

We identified clones with a 100% match at the nucleotide (nt) level to J9 and J8 in the stimulated PBMC repertoire (UMI counts of 9 and 14, respectively), and related clones identical in both unstimulated and stimulated PBMC repertoires throughout the various branches of the lineage (branch tips labeled J, Q, M, N and P in Figure 6A). Overall, the repertoire showed a rapid expansion of class switched IgG with numerous nt point mutations from germline VH, strongly suggesting both J8 (27 nt) and J9 (28 nt) plasmablasts derived from memory B cells from a prior infection, consistent with previous studies (Priyamvada et al., 2016; Xu et al., 2016). Among this acute-phase repertoire, we did observe less mutated IgG clones A (3 nt), B (5 nt), and C (5 nt) early in the lineage (Figure 6A), which could represent antibodies derived from a *de novo* immune response, or from less mutated memory clones. Finally, the divergent evolution of J9 and J8 suggested multiple somatic hypermutation pathways within this lineage leading to bNAbs.

VH and VL maturation contributes to broadly neutralizing activity

As described above, J8 and J9 VH derived from V-D-J recombination of IGHV1-69 with IGHD2-2 and IGHJ5. Although we did not analyze the light chain repertoires, both J8 and J9 used the same founder germline IGKV3-11 and IGKJ2 genes with identical CDR lengths and no convergent mutations from germline (Figure 6C). To investigate the contribution of somatic hypermutation (SHM) on broadly neutralizing activity, we generated a panel of recombinant IgG variants, confirmed proper folding (Figure S11), and tested them for neutralizing activity. As expected, recombinant J8 and J9 IgGs expressing fully germline VH and VL had no neutralizing activity (Figures 7A-D). Similarly, J8 and J9 IgG expressing germline VH paired with the corresponding mature VL, and vice versa, did not neutralize DENV1-4, suggesting that both VH and VL SHM contributed to neutralizing activity.

Several mutations occurred early in the J8/J9 lineage, including CDR-H2 I53F, CDR-H3 T99A/P and D100cH (clones labeled A, B, and C in Figure 6A, and alignments in Figure 6B), and were retained throughout the continued VH somatic hypermutation. To investigate the VH SHM requirements for broadly neutralizing activity, we generated “J9 5mut” and “J8 5mut” variants containing the above three early VH mutations (I53F, T99P, D100cH) and two additional CDR-H2 mutations (Q61D, K62N) common across different lineage branches (Figures 6A and 6B). We paired J8 and J9 5mut VH with the corresponding mature VL to generate recombinant IgGs. These five CDR-H2 and CDR-H3 mutations were sufficient for broadly neutralizing activity of J8 against DENV1-4 (Figures 7A-D) and of J9 against DENV1 and DENV2 only (Figures 7A-B). Compared to fully mature J9, J9 5mut displayed reduced neutralization potency against DENV3 and DENV4 (Figures 7C-D), suggesting that additional J9 VH mutations were required for

neutralization of these viruses. J9 VL mutations also played a role in neutralization of DENV3 and DENV4 as chimeric IgG expressing J9 heavy chain with J8 light chain displayed less potent neutralization of these viruses (Figures 7C-D). Finally, although the FR2 of J9 VH contained a glycine insertion not present in related clones (Figure 6B), this insertion was not necessary for neutralizing activity (Figure 7A-D).

Discussion

A safe and effective vaccine to protect against DENV remains elusive, largely due to the challenge of eliciting antibodies that can potently neutralize all four viral serotypes simultaneously to minimize the risk of ADE. For antigenically diverse viruses, more than one antibody specificity may be required to provide optimal coverage of diverse circulating variants (Bell et al., 2019; Doria-Rose et al., 2012; Goo et al., 2012; Katzelnick et al., 2015; Keeffe et al., 2018; Kong et al., 2015). Although cross-reactive antibodies against flaviviruses have been described, very few display potent neutralizing activity (Barba-Spaeth et al., 2016; Dejnirattisai et al., 2015; Xu et al., 2017). The epitope for one of these bNAbs (SiGN-3C) is not well defined but involves 2 residues within DII fusion loop and one in DIII (Xu et al., 2017). Detailed epitope mapping studies have been performed only for the EDE class of bNAbs, which recognize a quaternary epitope spanning both monomers within the E protein dimer (Barba-Spaeth et al., 2016; Rouvinski et al., 2015). This epitope involves five main regions on the E protein: *b* strand, fusion loop, and *ij* loop on DII; glycan loop on DI; and the DIII A strand. In this study, we functionally characterized 28 mAbs identified to be clonally expanded and somatically hypermutated by transcriptomic analyses of single plasmablasts from two individuals acutely infected with DENV (Zanini et al., 2018). Among these, we identified bNAbs J9 and J8, which potently neutralized all four DENV serotypes and recognize an epitope with major determinants in DI. The location of residues important for J9 and J8 recognition (Figure 5A), and the ability of these bNAbs to bind virus particles but not soluble E protein (Figure 1) suggest a quaternary epitope. Alternatively, the epitope may be localized to the E monomer, but is preferentially displayed on virus particles, as previously described for a DENV1-specific mAb (Fibriansah et al., 2014). Nevertheless, our epitope mapping results demonstrated that the recognition determinants for J9/J8 are distinct from EDE bNAbs because E protein mutations that reduced neutralization potency of J9/J8 either increased or did not alter neutralization potency of EDE1 and EDE2 antibodies, respectively (Figure 5). Thus, our study defines a new vulnerable site on the DENV E protein that can be exploited for immunogen design to elicit bNAbs.

A common strategy to isolate and characterize virus-specific mAbs involves sorting hundreds of single B cells from immune donors followed by reverse-transcription (RT)-PCR to isolate paired VH/VL genes for recombinant IgG production and functional characterization (Dejnirattisai et al., 2015; Robbiani et al., 2017; Rogers et al., 2017). In some cases, memory B cells that specifically bind viral antigens are first enriched by staining with fluorescently labeled antigen (Robbiani et al., 2017; Rogers et al., 2017; Scheid et al., 2009; Woda & Mathew, 2015; Wu et al., 2010). Alternatively, single B cells are cultured, and secreted antibodies are directly screened for function (Walker et al., 2009). Although these methods have successfully identified many human bNAbs, including those against flaviviruses (Dejnirattisai et al., 2015; Smith et al., 2013; Tsai et al., 2013; Xu et al., 2012; Xu et al., 2017), they involve labor intensive steps. Instead of screening a large panel of candidate antibodies, we leveraged transcriptomic

analyses of single plasmablasts from acute secondary DENV infection to focus our screen on clonally expanded and somatically hypermutated B cells (Zanini et al., 2018), which are likely to encode antigen-specific and affinity matured antibodies. Using this approach, we successfully identified highly potent mAbs capable of neutralizing all four DENV serotypes. It is unclear whether this bioinformatics-based approach to identify DENV bNAbs is fortuitous as acute DENV infection has been shown to induce a rapid and massive expansion of plasmablasts, many of which can neutralize multiple DENV serotypes (Priyamvada et al., 2016; Wrammert et al., 2012; Xu et al., 2012), or whether it is applicable to the rapid identification of highly functional antibodies against other viruses.

J9 and J8 are somatic IgG variants isolated from the same patient (013) who had an acute secondary infection with DENV4 (Zanini et al., 2018). NGS of the B cell repertoire and phylogenetic analysis of the J9/J8 lineage revealed divergent evolution of these bNAbs (Figure 6A), suggesting multiple SHM pathways to generate bNAbs against the J9/J8 epitope, which is encouraging for vaccine design. Antibody lineage divergence and parallel evolution leading to multiple bNAbs within the same individual has also been described in the context of HIV infection (MacLeod et al., 2016). J9 and J8 bNAbs derived from IGVH1-69 and IGVK3-11 germline genes. Consistent with a previous study of DENV-infected individuals (Appanna et al., 2016), many of the DENV-specific mAbs originating from plasmablasts of patient 013 also derived from IGVH1-69 (Table S3), which is commonly used among bNAbs against other viruses such as influenza and Hepatitis C virus (Chen, Tzarum, Wilson, & Law, 2019). Many of these bNAbs can achieve neutralization breadth and potency with limited SHM (Lingwood et al., 2012; Tzarum et al., 2019). Despite a moderately high degree of SHM for J8 VH (9.9% at the nucleotide level, Figure S1), five early amino acid mutations in CDR-H2 and CDR-H3 were sufficient for neutralization breadth and potency (Figure 7). As the paired VL had a low (1.4%) level of SHM, this observation suggests a relatively limited maturation pathway to a highly functional antibody.

To our knowledge, all human bNAbs against flaviviruses identified in the context of natural infection so far, including J9 and J8, were isolated from plasmablasts of individuals sequentially exposed to at least two different DENV serotypes (Dejnirattisai et al., 2015; Xu et al., 2012; Zanini et al., 2018). Sequential infection with heterologous DENV serotypes or HIV strains has been shown to broaden and strengthen the polyclonal neutralizing antibody response (Cortez, Odem-Davis, McClelland, Jaoko, & Overbaugh, 2012; Patel et al., 2017; Tsai et al., 2015; Tsai et al., 2013). One proposed model is that low affinity, cross-reactive antibody secreting B-cell clones elicited by primary DENV exposure are reactivated during secondary infection to undergo further affinity maturation resulting in antibodies with more broad and potent neutralizing activity (Patel et al., 2017). Although the relatively high level of SHM already present in J9 and J8 at day 4 post-fever onset following secondary DENV infection suggests a recall response, repertoire analysis from earlier time points would be required to determine whether the memory B cell clones from which these bNAbs were derived underwent further SHM to achieve neutralization breadth and potency.

It is also unclear whether the specificities and functions of plasmablast-derived mAbs present during acute infection confer long-lived protection from infection and pathogenesis. Interestingly, despite the presence of plasmablast-derived bNAbs such as J9 and J8, and those belonging to the EDE class during acute secondary infection, the donors from which these antibodies were isolated subsequently developed severe dengue disease (Dejnirattisai et al., 2015; Zanini et al., 2018). Indeed, the rapid and massive plasmablast activation following acute DENV infection is coincident with the onset of severe symptoms and has been proposed to contribute to immunopathology (Wrammert et al., 2012). Alternatively, despite broad and potent *in vitro* neutralizing activity against a surrogate panel of DENV1-4 strains, these bNAbs may not efficiently neutralize circulating infecting strains. Finally, it is possible that these bNAbs make up a minor component of the overall polyclonal antibody response, as supported by our finding that J9/J8-like mAbs minimally contribute to the overall neutralizing activity of patient 013 serum (Figure S9). Moreover, BCR repertoire analysis revealed that though expanded, the J9/J8 clonal family is not the largest in this donor (Table S3), at least not in the acute phase sample tested. The complex interplay among B cells and antibodies of different specificities and functions present in sera, and their impact on immunity and pathogenesis warrant further study.

Acknowledgements

We thank the cohort participants and staff; Ted Pierson for providing Raji-DCSIGNR cells and constructs for RVP production; Anna Sellas, Gorica Margulis, Esther Ho, and Purnima Ravisankar for lab management and support; Peter Kim and Don Ganem for helpful discussion; Erick Matsen and Duncan Ralph for valuable comments on the manuscript.

Molecular graphics and analyses of the DENV2 E dimer were performed with UCSF Chimera, developed by the Resource for Biocomputing, Visualization, and Informatics at the University of California, San Francisco, with support from NIH P41-GM103311.

This work was funded by the Chan Zuckerberg Biohub (NDD, AA, EW, FZ, OS, EC, JEP, SRQ, KMM, LG); NSF Graduate Research Fellowship and the Kou-I Yeh Stanford Graduate Fellowship (DC); Catalyst Award from Dr. Ralph & Marian Falk Medical Research Trust and the Stanford Bio-X Interdisciplinary Initiatives Seed Grants Program (SE); Stanford Advanced Residency Training at Stanford Fellowship Program (MR); NIH contract HHSN272201400058C (BJD); and Fred Hutchinson Cancer Research Center (LG).

Competing interests

FZ, DC, MR, LG, SRQ, SH, KMM, and EW are inventors of the following patent application, which is co-owned by the Chan Zuckerberg Biohub and Stanford University: PCT patent application entitled ANTIBODIES AGAINST DENGUE VIRUS AND RELATED METHODS, Serial no. PCT/US2019/045427, filed August 7, 2019.

Methods

Patient samples

The study was approved by the Stanford University Administrative Panel on Human Subjects in Medical Research (Protocol #35460) and the Fundación Valle del Lili Ethics committee in biomedical research (Cali,Colombia). All subjects, their parents, or legal guardians provided written informed consent, and subjects between 6 to 17 years of age and older provided assent. We collected blood samples from individuals who presented with symptoms compatible with dengue between 2016 and 2017 to the Fundación Valle del Lili in Cali, Colombia. Cohort details have been previously described (Zanini et al., 2018).

Monoclonal antibodies

Plasmablast-derived variable heavy or light chain sequences (Zanini et al., 2018) were synthesized as gene fragments (Genewiz, San Francisco, CA; Integrated DNA Technologies, Coralville, IA) to include at least a 15 basepair overlap with the 5' signal sequence and 3' constant region of our human IgG1, kappa or lambda expression vectors described elsewhere (Waltari et al., 2019). For pilot ELISAs and neutralization assays using crude IgG-containing supernatant, paired heavy and light chain plasmids for each mAb were expressed in Expi293F cells (Cat# A14527, ThermoFisher Scientific, Waltham, MA) in a 96-well format. IgG levels were quantified by ELISA as described (Waltari et al., 2019). Antibodies with crude IgG expression levels < 0.5 ng/mL were excluded from further characterization. Antibodies selected for in-depth characterization (J9, J8, C4, B10, M1, L8 and I7), as well as control mAbs EDE1 C10 (Dejnirattisai et al., 2015), EDE2 B7 (Dejnirattisai et al., 2015), CR4354 (Kaufmann et al., 2010) were expressed by transient transfection of Expi-CHO-S cells (Cat# A29129; ThermoFisher Scientific). Variable heavy and light chain sequences of the above control mAbs used for gene synthesis and cloning into expression vectors were based on PDB IDs 4UT9, 4UT6, and 3N9G, respectively. Cell culture supernatant was clarified by centrifugation at 3900 xg for 30 min at 4°C, passed through a 0.22 µm filter, and IgG was purified on MabSelect SuRe resin (Cat# 17-5438-01; GE Healthcare, Chicago, IL). Other control mAbs used in this study were obtained commercially: Anti-Dengue Virus Type II Antibody, clone 3H5-1 (Cat# MAB8702; Millipore Sigma, Burlington, MA); Flavivirus group antigen Antibody (D1-4G2-4-15 (4G2)) (Cat# NBP2-52709-0.2mg; Novus Biologicals, Centennial, CO).

Cells

Expi293F cells (Cat# A14527; ThermoFisher Scientific) were cultured in Expi293 Expression Medium (Cat# A1435101; ThermoFisher Scientific) according to the manufacturer's instructions. Expi-CHO-S Cells (Cat# A29127; ThermoFisher Scientific) were cultured in ExpiCHO Expression Medium (Cat# A2910001; ThermoFisher Scientific). HEK-293T/17 cells (ATCC CRL-11268) were maintained in DMEM (Cat# 11965118; ThermoFisher Scientific) supplemented with 10% fetal bovine serum (Cat# FB-11; Omega Scientific, Inc.) and 100U/mL penicillin-streptomycin (Cat# 15140-122; ThermoFisher Scientific). Raji cells stably expressing DCSIGNR (Raji-DCSIGNR) (Davis et al., 2006) (provided by Ted Pierson, NIH) and K562 cells (ATCC Cat# CCL-243) were maintained in RPMI 1640 supplemented with GlutaMAX (Cat# 72400-047; ThermoFisher Scientific), 10% FBS and 100U/mL penicillin-streptomycin. All cells

were maintained at 37°C in 5% CO_2 unless otherwise stated. C6/36 cells (ATCC CRL-1660) were maintained in EMEM (ATCC Cat# 30-2003) supplemented with 10% FBS at 30°C in 5% CO_2.

Production of reporter virus particles (RVPs)

RVPs were produced by co-transfection of HEK-293T/17 cells with (i) a plasmid expressing a WNV subgenomic replicon encoding GFP in place of structural genes (Pierson et al., 2006), and (ii) a plasmid encoding C-prM-E structural genes from the following viruses: DENV1 Western Pacific (WP) (Ansarah-Sobrinho, Nelson, Jost, Whitehead, & Pierson, 2008), DENV2 16681 (Ansarah-Sobrinho et al., 2008), WNV NY99 (Pierson et al., 2006), and ZIKV H/PF/2013 (Dowd et al., 2016). Briefly, 8 x 10^5 HEK-293T/17 cells pre-plated in a 6-well plate were co-transfected with a mass ratio of 1:3 replicon:C-prM-E plasmids using Lipofectamine 3000 (Cat# L3000-015; ThermoFisher Scientific). Four hours post-transfection, media was replaced with low-glucose DMEM (Cat# 12320-032; ThermoFisher Scientific) containing 10% FBS and 100U/mL penicillin-streptomycin (i.e. low-glucose DMEM complete) and cells were transferred to 30°C in 5% CO_2. RVP-containing supernatant was harvested at 3, 4, and 5 days post-transfection, passed through a 0.22 µm filter, pooled, and stored at -80°C. DENV3 strain CH53489 RVPs (Cat# RVP-301; Integral Molecular, Philadelphia, PA) and DENV4 strain TVP360 RVPs (Cat# RVP-401; Integral Molecular) were obtained commercially. RVPs with increased efficiency of prM cleavage were produced as above by co-transfecting plasmids encoding the replicon, structural genes, and human furin (provided by Ted Pierson, NIH) at a 1:3:1 mass ratio. Where indicated, RVPs were concentrated by ultracentrifugation through 20% sucrose at 164,000 xg for 4 h at 4°C, resuspended in HNE buffer (5mM HEPES, 150mM NaCl, 0.1mM EDTA, pH 7.4), and stored at -80°C.

Infectious titers of RVPs were determined by infection of Raji-DCSIGNR cells. At 48 h post-infection, cells were fixed in 2% paraformaldehyde (Cat# 15714S; Electron Microscopy Sciences, Hatfield, PA), and GFP positive cells quantified by flow cytometry (Intellicyt iQue Screener PLUS, Sartorius AG, Gottingen, Germany).

Production, titer and neutralization of fully infectious contemporary DENV1-4 isolates

The following DENV contemporary strains were used to infect C6/36 cells: DENV1 UIS 998 (Cat# NR-49713; BEI), DENV2 US/BID-V594/2006 (Cat# NR-43280; BEI), DENV3/US/BID-V1043/2006 (Cat# NR-43282; BEI), DENV4 Strain UIS497 (Cat# NR-49724; BEI). Virus-containing supernatant was collected at days 2-7 post-infection, filtered, and stored at -80 °C. Infectious titer was determined on Raji-DCSIGNR cells. At 48 h post-infection, intracellular staining was performed using BD Cytofix/Cytoperm Solution Kit (Cat# 554714; BD Biosciences, San Jose, CA) according to the manufacturer's instructions. Mouse mAb 4G2 conjugated to Alexa Fluor 488 (Cat# A20181; Thermo Fisher Scientific) was used for intracellular staining to detect infected cells by flow cytometry (Intellicyt iQue Screener PLUS, Sartorius AG). Neutralization assays were performed as described below, using intracellular staining with Alexa Fluor 488-conjugated 4G2 to detect infected cells.

Generation of E protein variants

The DENV2 16681 C-prM-E expression construct (Ansarah-Sobrinho et al., 2008) was used as a template for site-directed mutagenesis using the *Pfu* Ultra DNA polymerase system (Cat# 600380; Agilent Technologies, Santa Clara, CA) and primers generated by QuikChange® Primer Design (Agilent Technologies). The entire C-prM-E region was sequenced (Quintara, San Francisco, CA) to confirm the presence of the desired mutation(s).

Shotgun mutagenesis epitope mapping

A DENV2 strain 16681 prM/E expression construct was subjected to high-throughput shotgun mutagenesis to generate a comprehensive mutation library, with each prM/E polyprotein residue mutated to alanine (with alanine residues to serine). In total, 559 DENV2 mutants were generated (99.6% coverage of the prM/E protein), sequence confirmed, and arrayed into 384-well plates (one mutation per well). For mAb library screening, plasmids encoding the DENV protein variants were transfected individually into human HEK-293T cells and allowed to express for 22 h before fixing cells in 4% paraformaldehyde (Electron Microscopy Sciences), and permeabilizing with 0.1% (w/v) saponin (Sigma-Aldrich, St. Louis, MA) in PBS plus calcium and magnesium (PBS++). Cells were incubated with purified mAbs (0.1-2.0 µg/mL) diluted in 10% NGS (Sigma-Aldrich) / 0.1% saponin, pH 9.0. MAb J9 was screened in unfixed cells that had been co-transfected with the prM/E library and furin expression plasmids, to decrease levels of prM in the cells. Before screening, the optimal concentration was determined for each antibody, using an independent immunofluorescence titration curve against wild-type prM/E to ensure that signals were within the linear range of detection and that signal exceeded background by at least 5-fold. Antibodies were detected using 3.75 µg/mL Alexa Fluor 488-conjugated secondary antibody (Jackson ImmunoResearch, West Grove, PA) in 10% NGS / 0.1% saponin. Cells were washed three times with PBS++ / 0.1% saponin followed by 2 washes in PBS. Mean cellular fluorescence was detected using a high throughput flow cytometer (Intellicyt iQue Screener Plus, Sartorius AG). Antibody reactivity against each mutant protein clone was calculated relative to reactivity with wild-type prM/E, by subtracting the signal from mock-transfected controls and normalizing to the signal from wild-type protein-transfected controls. The entire library data for each mAb was compared to the equivalent data from control mAbs. Mutations were identified as critical to the mAb epitope if they did not support reactivity of the test mAb (<20% of reactivity to WT prM/E) but supported reactivity of appropriate control antibodies (>70% of reactivity to WT prM/E). This counter-screen strategy facilitates the exclusion of DENV prM/E protein mutants that are mis-folded or have an expression defect (Davidson & Doranz, 2014; Paes et al., 2009).

ELISA

High-binding 96-well plates (Cat# CLS3361; Millipore Sigma, Burlington, MA) were either coated directly with 500 ng/well of recombinant DENV2 16681 E protein (Cat# DENV2-ENV-500; The Native Antigen Company, Oxford, UK) or with 300 ng/well of murine mAb 4G2 for capture of concentrated and partially purified RVPs. Recombinant E or capture mAb was added in 100 µl 1X PBS and incubated at 4°C overnight. The following day, 300 µl 1% BSA in PBS blocking buffer (Cat# B0101; Teknova, Hollister, CA) was added for 1 h either at room temperature (RT) or 37°C. Plates were subsequently washed 6 times using 300 µl PBST (PBS + 0.05% Tween-20) and 100 µl of DENV2 RVPs diluted 1:10 in blocking buffer was added to wells coated with

murine mAb 4G2 and incubated for 1 hr at RT and 37°C. Plates were washed 6 times and incubated with 5 µg/well of primary mAbs in 100µl blocking buffer for 1 h at room temperature or 37°C. Plates were washed 6 times and incubated with horseradish peroxidase (HRP)-conjugated mouse anti-human IgG Fc secondary antibody (Cat# 05-4220; ThermoFisher Scientific) diluted 1:1000 in 100 µl blocking buffer for 1 h at room temperature or 37°C. Plates were washed 6 times, and 100 µl TMB substrate (Cat# 34028; Thermo Fisher Scientific) was added at room temperature. The reaction was stopped after 6 min by adding 50 µl of 1N HCL. The absorbance at 450 nm was determined using a microplate reader (SpectraMax i3, Molecular Devices, San Jose, CA).

Protein array printing and ELISA

Spotted protein arrays (5 x 6) were printed onto each well of Greiner high-binding 96-well plates (Cat# 655097, Thermo Fisher Scientific) using a sciFLeXARRAYER S12 (Scienion AG, Berlin). An array with 75x final concentration of sucrose-purified DENV2 RVPs and a final concentration of 180 µg/mL of recombinant DENV2 16681 E protein was printed alongside 10 µg/mL anti-human IgG Fc (Cat# 09-005-098; Jackson ImmunoResearch), and 1 µg/mL biotinylated kappa secondary (Cat# 2060-08, SouthernBiotech, Birmingham, AL). Probes were diluted 1:1 with D12 buffer (Cat# CBP-5436-25; Scienion AG) and printed at the final concentrations indicated above in triplicate spots from a 384-well source plate (Cat# CPG-5502-1; Scienion AG) chilled to dew point with 3 x 350 pL drops per spot at 60% humidity on each 96-well plate. Plates were cured overnight at 70% humidity before vacuum sealing.

For ELISAs, printed 96-well plates were washed once with binding buffer (0.5% BSA + 0.025% Tween in PBS) then blocked in 100 µl/well blocking buffer (3% BSA in PBS + 0.05% Tween-20 (PBST)). After 1 h, blocking buffer was removed and 100 µl/well of test mAbs diluted in binding buffer added and incubated overnight at 4°C. We tested twelve 3-fold serial dilutions of J9, J8, C4, EDE1 C10, EDE2 B7 and CR4354 starting at 200 µg/mL; and B10, M1, L8 and I7 starting at 2 µg/mL. The following day, plates were washed 3 times with PBST, and 100 µl/well of goat anti-human IgG Fc-BIOT (Cat# 2014-08; Southern Biotech) secondary antibody diluted 1:10,000 in binding buffer was added. After 1 h shaking incubation at room temperature, plates were washed 3 times, followed by 1 h shaking incubation at room temperature with 100 µl/well Pierce High Sensitivity Streptavidin-HRP (Cat# 21130, Thermo Fisher Scientific). Plates were again washed 3 times, developed for 20 min with 50 µl/well SciColor T12 (Cat# CD-5600-100; Scienion AG), then analyzed using sciREADER CL2 (Scienion AG). Dose-response binding curves were analyzed by non-linear regression with a variable slope (GraphPadPrism v8, GraphPad Software Inc., San Diego, CA).

Neutralization and antibody-dependent enhancement assays

RVP stocks diluted to 5-10% final infectivity were incubated with 5-fold dilutions of mAb or heat-inactivated (65°C for 30 min) serum for 1 h at room temperature before addition of Raji-DCSIGNR cells (neutralization assays) or K562 cells (ADE assays). After 48 h incubation at 37°C, cells were fixed in 2% paraformaldehyde and GFP positive cells were quantified by flow cytometry (Intellicyt iQue Screener Plus, Sartorius AG). Dose-response neutralization curves were analyzed by non-linear regression with a variable slope (GraphPadPrism v8, GraphPad

Software Inc.). Fab fragments were generated and purified from IgGs using the Pierce Fab Preparation Kit (Cat# PI44985; Thermo Scientific) and used in neutralization assays at 2x molar concentration relative to IgG.

Pre- and post-attachment neutralization assays were carried out as previously described (Xu et al., 2017) using Raji-DCSIGNR cells, DENV2 RVPs, and serial 5-fold dilutions of mAb starting at 150 µg/mL (J9 and J8) or 300 µg/mL (C4 and EDE1 C10). All cells, RVPs, mAbs, and media were pre-chilled to 4°C prior to use. For the pre-attachment assay, mAb dilutions were mixed with undiluted DENV2 RVPs for 1 h at 4°C followed by the addition of Raji-DCSIGNR cells and incubation for 1 h at 4°C. Cells were washed 3 times with media, resuspended in media and incubated for 48 h at 37°C. For the post-attachment assay, undiluted DENV2 RVPs were incubated with Raji-DCSIGNR cells for 1h at 4°C, washed three times with media, resuspended in fresh media and incubated with antibody dilutions. After 1 h at 4°C, cells were washed three times with media, resuspended in media and incubated for 48 h at 37°C. After 48 h at 37°C, cells from both pre- and post-attachment assays were fixed in 2 % paraformaldehyde. GFP positive cells were quantified by flow cytometry after 48h incubation, as described above.

Preparation of PBMCs for BCR repertoire analysis

A 1 ml vial of PBMCs was thawed rapidly in a 37°C water bath, immediately diluted into 9 ml of B cell growth media containing Corning® DMEM [+] 4.5 g/L glucose, sodium pyruvate [-] L-glutamine (VWR International, Radnor, PA), 1x Pen/Strep/Glu and 10% ultralow IgG HI-FBS (Thermo Fisher Scientific), and pelleted at 350 xg for 5 min. The cells were resuspended in 1 mL of growth media and filtered through a 5 ml polystyrene tube with a cell strainer cap (Thomas Scientific, Swedesboro, NJ). One half of the PBMCs were transferred to the T25 flask with feeder cells and B cell stimulation media as described previously (Waltari et al., 2019) and the other half was spun down in a 1.5 ml Eppendorf tube at 8000 rpm for 5 min, resuspended in 600 µl RLT (Qiagen, Hilden, Germany) + beta-mercaptoethanol, allowed to lyse for 5 min, snap frozen on dry ice and stored at -80°C until RNA purification with the Qiagen AllPrep RNA/DNA kit (Qiagen). Immunoglobulin amplicon preparation, sequencing and BCR analysis were previously described (Waltari et al., 2019). Lineage trees were constructed using the IgPhyML package in the Immcantation pipeline (Hoehn, Fowler, Lunter, & Pybus, 2016) to construct a somatic hypermutation-optimized maximum likelihood phylogeny of the heavy chain sequences clonally related to J9 and J8.

Figure legends

Figure 1. Binding profile of mAbs. A single dilution of the mAbs indicated on the x-axis was tested for binding to DENV2 **(A)** soluble recombinant E protein (rE) and **(B)** reporter virus particles (RVPs) at room temperature (RT) and 37°C by ELISA. The y-axis shows absorbance values at 450 nm. Error bars indicate the range of values obtained in duplicate wells. Data are representative of 3 independent experiments. The dotted horizontal line in (B) indicates the average A450 values obtained for negative control WNV-specific mAb CR4354. Representative dose-response binding curves of the indicated mAbs to DENV2 **(C)** rE and **(D)** RVPs at room temperature. The y-axis shows binding signal intensity in arbitrary units (AU). Error bars indicate the standard deviation (SD) of triplicate spots within one well of the microarray. Binding curves are representative of two independent experiments.

Figure 2. Neutralization profile of mAbs. (A) Representative mAb dose-response neutralization curves against DENV1-4, ZIKV, and WNV RVPs. Infectivity levels were normalized to those observed in the absence of antibody. Data points and error bars indicate the mean and range, respectively. Results are representative of at least 3 independent experiments, each performed in duplicate. **(B)** MAb concentrations resulting in 50% inhibition of infectivity (IC_{50}) from dose-response neutralization experiments described in (A). Values represent the mean of at least 3 independent experiments, each performed in duplicate. The heatmap indicates neutralization potency, as defined in the key. Grey boxes indicate that 50% neutralization was not achieved at the highest mAb concentration tested (10 μg/ml). The patient (Pt) from which mAbs were isolated are indicated above each mAb name. MAbs from shared clonal families are indicated.

Figure 3. Mechanism of neutralization. Representative dose-response curves for pre- and post-attachment neutralization of DENV2 16681 RVPs by the indicated mAbs. Results are representative of at least 2 independent experiments each performed in duplicate. Data points and error bars indicate the mean and range, respectively.

Figure 4. Critical E protein residues for mAb binding. Individual alanine mutation of a subset of DENV2 E residues decreased binding by mAbs **(A)** M1 and L8, **(B)** I7 or **(C)** J9 as shown, but did not affect binding by other mAbs, including EDE1 C10 and a previously screened control mAb (FL) targeting the fusion loop (unpublished). Error bars represent the mean and range (half of the maximum-minus-minimum values) of at least two biological replicates. The dotted horizontal line indicates 80% reduction in mAb binding reactivity to mutant compared to wildtype DENV2 E. Above each graph, residues involved in binding of the corresponding mAb are highlighted on the ribbon structure of one of the monomers (black) within the DENV2 E dimer (PDB: 1OAN). Residues in DI, DII, DIII, and DII fusion loop are indicated in red, yellow, blue, and green, respectively.

Figure 5. Critical E protein residues for mAb neutralization. (A) Ribbon structure of the DENV2 E dimer (PDB: 1OAN) with one monomer in black and the other in grey. The conserved DII fusion loop is shown in green. Colored spheres indicate residues that contribute to J9 recognition identified in Figure S8A and summarized in (B). Bar graphs depict the mean fold change in IC_{50} values against the DENV2 E variants indicated on the x-axis relative to DENV2 wildtype RVPs for mAbs **(B)** J9, **(C)** J8, **(D)** C4, **(E)** EDE1 C10, and **(F)** EDE2 B7. For each mAb, wildtype ZIKV RVPs were included as controls. Mean values were obtained from 2 to 7 independent experiments represented by data points. Error bars indicate the standard deviation ($n > 2$ experiments) or range ($n = 2$ experiments). Bar colors correspond to those of spheres in

(A) to indicate location within the E dimer. The dotted horizontal line indicates a 4-fold increase in IC_{50} value relative to wildtype DENV2.

Figure 6. Lineage analysis of the J9/J8 clonal family. (A) Maximum likelihood phylogeny of mAbs related to J9 and J8 found in the BCR repertoire of patient 013 created using the HLP19 model in IgPhyML. VH germline sequence (IGHV1-69*05 + IGHD2-2 + IGHJ5) is shown at the top. Red letters and tips indicate sequences found in unstimulated PBMCs, black letters and tips indicate sequences found in stimulated PBMCs, and magenta letters indicate sequences found both in unstimulated and stimulated PBMCs. Letters correspond to sequences shown in the alignment in (B). Triangles next to tips indicate IgA sequences. (**B**) Heavy chain alignment of selected mAbs within the J9/J8 lineage found in the BCR repertoire of patient 013. Letters correspond to sequences shown in (A), with isotype indicated. The germline sequence (IGHV1-69 + IGHD2-2 + IGHJ5) is shown first, followed by a constructed sequence with 5 amino acid changes shown as “GERM 5mut.” Kabat numbering is shown on top. Amino acid changes are highlighted in gray, and boxes indicate the CDR regions. (**C**) Light chain alignment of J8 and J9. The germline sequence (IGKV3-11 + IGKJ2) is shown first, with Kabat numbering shown on top. Amino acid changes are highlighted in gray, and boxes indicate the CDR regions.

Figure 7. Contribution of VH and VL SHM to J9 and J8 neutralizing activity. Summary of IC_{50} values of J9 and J8 IgG variants against **(A)** DENV1, **(B)** DENV2, **(C)** DENV3, and **(D)** DENV4 RVPs. Bars represent mean IC_{50} values obtained from 3 to 4 independent experiments indicated by data points for each mAb. Error bars show the SD. Values at the dotted horizontal line indicates that 50% neutralization was not achieved at the highest IgG concentration tested (10 µg/ml). IC_{50} values for fully mature J9 and J8 are shown in red and blue bars, respectively. J8J9_full germ: germline J8/J9 heavy chain (HC) paired with J8/J9 light chain (LC); J9_HCgerm: J9 germline HC paired with J9 mature LC; J9LC_germ: J9 mature HC paired with J9 germline LC; J8_HCgerm: J8 germline HC paired with J8 mature LC; J8_LCgerm: J8 mature HC paired with J9 germline LC; J9_HC5mut: J9 HC with 5 mutations indicated in Figure 6B paired with J9 mature LC; J8_HC5mut: J8 HC with 5 mutations indicated in Figure 6B paired with J8 mature LC; J9HC_J8LC: J9 mature HC paired with J8 mature LC; J8HC_J9LC: J8 mature HC paired with J9 mature LC; J9 -G: J9 HC with a single glycine deletion in FR2 paired with mature J9 LC.

Supplemental Information

Table S1. Percent mAb binding reactivity to DENV2 E protein alanine scanning mutagenesis library normalized to wildtype DENV2

Table S2. Summary of Ig sequences, clonal families, and mean SHM in unstimulated versus stimulated PBMCs from patient 013.

Table S3. Sequences from patient 013 unstimulated and stimulated PBMCs related to clonal families of single plasmablasts with reactivity to DENV

Figure S1. Characteristics of plasmablast-derived mAbs from DENV-infected patients. MAb sequences were identified from single plasmablasts of DENV-infected patient 013 and patient 020, as previously described (Zanini et al., 2018). The patient from which corresponding mAb sequences were identified is listed in the first column, followed by mAb clonal family ID, mAb name, and gene usage, % nucleotide (nt) SHM, and CDR3 amino acid (aa) length for the variable heavy (VH) and light (VL) chain genes. VH and VL sequences were cloned into IgG1 expression vectors and transfected into mammalian cells. Neat crude IgG1-containing culture supernatant was tested for binding to recombinant DENV2 E protein ectodomain and DENV2 RVPs by ELISA, and for neutralizing activity against the indicated RVPs. MAbs 3H5-1 (2 µg/mL), EDE2 B7(2 µg/mL) and EDE1 C10 (10 µg/mL), and CR4354 (2 µg/mL) were used as controls. MAb binding activity is expressed as fold-change in absorbance values over negative control wells containing media only. The heatmap (light to dark blue) indicates strength of binding, as defined in the key below the table. A value of 1 indicates no increase in binding relative to negative control wells. Percent neutralization was calculated using the formula: (% infection in the absence of IgG1 - % infection in the presence of IgG1) / (% infection in the absence of IgG1) x 100. The heatmap (yellow to red) indicates the range of neutralization potencies as indicated in the key below the table. Results are representative of 2 independent experiments. Under the crude IgG column, a value of <0.0005 indicates undetectable levels of IgG1 in crude culture supernatant. Antibodies selected for further characterization are shown in bold. “N/a,” not applicable; “nc,” not successfully cloned; “nd,” not determined.

Figure S2. Neutralization potency of IgG and Fab fragments. (A) J9, **(B)** J8, **(C)** C4, and **(D)** EDE1 C10 were tested as Fab fragments or full-length IgG for neutralization of DENV2 RVPs. Dose-response neutralization curves represent 3 independent experiments, each performed in duplicate. Data points and error bars indicate the mean and range, respectively. **(E)** Mean IC_{50} values of the indicated IgG or Fab fragment from 3 independent experiments represented by data points. Error bars represent the SD. Values at the dotted horizontal line indicates that 50% neutralization was not achieved at the highest concentration of IgG or Fab tested. Fabs were tested at 2x excess molar concentration relative to IgG.

Figure S3. Neutralization potency of mAbs against contemporary DENV1-4 strains. Neutralization of contemporary DENV1-4 strains by **(A)** J9, C4, and **(B)** J8 was determined by intracellular staining with AF488-conjugated 4G2 at 48 h post-infection. Error bars indicate the range of duplicate infections. Infectivity levels were normalized to those in the absence of neutralizing antibody. Dose-response neutralization curves represent one experiment.

Figure S4. mAb neutralization of standard and mature RVP preparations. (A) Dose-response neutralization curves for the indicated mAbs against DENV2 RVPs prepared under standard conditions (Std) or in the presence of overexpressed furin to generate mature RVPs (Furin). Data points and error bars indicate the mean and range of infectivity in duplicate wells,

respectively. **(B)** Mean IC_{50} values of mAbs against standard or mature RVPs from 3 independent experiments depicted by data points. Error bars indicate the SD. P-values were obtained from two-tailed paired t-tests.

Figure S5. Antibody-dependent enhancement (ADE) of DENV2, ZIKV and WNV infection. Serial dilutions of the indicated mAbs were tested for ADE of **(A)** DENV2, **(B**) ZIKV or **(C)** WNV RVP infection of K562 cells. Error bars indicate the mean of infection in duplicate wells. Bar graphs represent average mAb concentrations at peak enhancement of **(D)** DENV2, **(E)** ZIKV or **(F)** WNV RVP infection obtained from 2-3 independent experiments, each represented by a data point. Where indicated, error bars represent the SD.

Figure S6. DENV2 E protein mutagenesis. (A) Alignment of DENV1-4, ZIKV, and WNV E ectodomain amino acid residues obtained using ClustalW2. Red, yellow, green, and blue bars above the alignment indicate residues within E protein DI, DII, DII-fusion loop, and DIII, respectively. Squares above colored bars indicate residues selected for mutagenesis and generation of RVP variants tested for sensitivity to J9 neutralization: gray squares = no effect on neutralization sensitivity; black squares = reduced sensitivity to J9 neutralization. Yellow squares indicate residues conserved across flaviviruses and important for mAb I7 binding. The sequence used for ZIKV H/PF/2013 differs at two amino acids (residue 246 K>R and 345 M>I from GenBank accession number AHZ13508.1, as previously described (Dowd et al., 2016). **(B)** Ribbon structure of the DENV2 E dimer (PDB 1OAN) with 34 individually mutated residues shown as gray spheres. E protein domains are color-coded as in (A). **(C)** Ribbon structure of the DENV2 E dimer (PDB 1OAN) with one monomer shown in black, and the other in gray. Colored spheres indicate the locations of paired mutations: K47T+V151T (red); L56V+Q211E (orange); E85Q+Q86S (green); H149S+V151T (blue); Y178F+M287V (cyan); N194S+E195D (purple); Q316L+K394S (yellow).

Figure S7. Infectious titer of DENV2 RVPs encoding E protein mutations. Infectious titers of DENV2 RVP encoding **(A)** single or **(B)** double E protein mutations. For each graph, white bars show the infectious titer of WT DENV2 RVP, and red, yellow, and blue bars represent mutations in DI, DII, and DIII, respectively. In (B), the purple bar represents a paired mutation at one residue in DI (Y178F) and another in DIII (M297V). Titers are based on one or two independent RVP preparations, as indicated by data points. Where present, error bars represent the range of infectivity from 2 independent RVP preparations.

Figure S8. Effect of E protein mutations mAb neutralization potency. We screened a panel of DENV2 RVP variants encoding single (left) or double (right) E protein mutations for sensitivity to neutralization by mAbs **(A)** J9, **(B)** J8, **(C)** C4, **(D)** EDE1 C10, and **(E)** EDE2 B7. Bar graphs represent average fold-change in IC_{50} relative to WT DENV2 RVP obtained from at least 2 independent experiments, as indicated by data points. Error bars indicate the range (n = 2) or SD (n > 2). The dotted line represents a 4-fold increase in IC_{50} relative to DENV2 WT. On the left panel, red, yellow, and blue bars indicate mutations are residues in DI, DII, and DIII, respectively. For each mAb, neutralization of WT ZIKV RVPs is included as a control.

Figure S9. Effect of E protein mutations on patient 013 serum neutralization potency. Neutralizing activity of mAb J9 and longitudinal serum samples from patient 013 were tested against DENV2 RVP variants encoding E protein mutations that reduced J9 neutralization potency. ZIKV WT RVP was included as a control. Serum samples 013-1, 013-2 and 013-3 were collected 4, 8 and 22 days after onset of fever, respectively. Dose-response neutralization curves are representative of 3 independent experiments, each performed in duplicate. Error bars indicate the range of infectivity normalized to infection levels in the absence of antibody.

Figure S10. Patient 013 VH gene usage. Germline VH gene usage among the unstimulated (circles) and stimulated (triangles) PBMC repertoires of patient 013, with only IgM (top) and IgG (bottom) sequences shown. Genes are grouped by color into gene families, as indicated in the key.

Figure S11. Analytical size exclusion chromatography of recombinant IgGs. Biophysical characterization of J9 and J8 IgG variants by analytical size exclusion chromatography (Superdex S200 Increase 3.2/300). A single major peak at 280 nm corresponding to monomeric IgG is observed.

References

Ansarah-Sobrinho, C., Nelson, S., Jost, C. A., Whitehead, S. S., & Pierson, T. C. (2008). Temperature-dependent production of pseudoinfectious dengue reporter virus particles by complementation. *Virology, 381*(1), 67-74. doi:10.1016/j.virol.2008.08.021

Appanna, R., Kg, S., Xu, M. H., Toh, Y. X., Velumani, S., Carbajo, D., . . . Fink, K. (2016). Plasmablasts During Acute Dengue Infection Represent a Small Subset of a Broader Virus-specific Memory B Cell Pool. *EBioMedicine, 12*, 178-188. doi:10.1016/j.ebiom.2016.09.003

Barba-Spaeth, G., Dejnirattisai, W., Rouvinski, A., Vaney, M. C., Medits, I., Sharma, A., . . . Rey, F. A. (2016). Structural basis of potent Zika-dengue virus antibody cross-neutralization. *Nature, 536*(7614), 48-53. doi:10.1038/nature18938

Bell, S. M., Katzelnick, L., & Bedford, T. (2019). Dengue genetic divergence generates within-serotype antigenic variation, but serotypes dominate evolutionary dynamics. *Elife, 8*. doi:10.7554/eLife.42496

Bhatt, S., Gething, P. W., Brady, O. J., Messina, J. P., Farlow, A. W., Moyes, C. L., . . . Hay, S. I. (2013). The global distribution and burden of dengue. *Nature, 496*(7446), 504-507. doi:10.1038/nature12060

Boonyaratanakornkit, J., & Taylor, J. J. (2019). Techniques to Study Antigen-Specific B Cell Responses. *Front Immunol, 10*, 1694. doi:10.3389/fimmu.2019.01694

Chen, F., Tzarum, N., Wilson, I. A., & Law, M. (2019). VH1-69 antiviral broadly neutralizing antibodies: genetics, structures, and relevance to rational vaccine design. *Curr Opin Virol, 34*, 149-159. doi:10.1016/j.coviro.2019.02.004

Cherrier, M. V., Kaufmann, B., Nybakken, G. E., Lok, S. M., Warren, J. T., Chen, B. R., . . . Fremont, D. H. (2009). Structural basis for the preferential recognition of immature flaviviruses by a fusion-loop antibody. *EMBO J, 28*(20), 3269-3276. doi:10.1038/emboj.2009.245

Cortez, V., Odem-Davis, K., McClelland, R. S., Jaoko, W., & Overbaugh, J. (2012). HIV-1 superinfection in women broadens and strengthens the neutralizing antibody response. *PLoS Pathog, 8*(3), e1002611. doi:10.1371/journal.ppat.1002611

Corti, D., & Lanzavecchia, A. (2014). Efficient Methods To Isolate Human Monoclonal Antibodies from Memory B Cells and Plasma Cells. *Microbiol Spectr, 2*(5). doi:10.1128/microbiolspec.AID-0018-2014

Crank, M. C., Ruckwardt, T. J., Chen, M., Morabito, K. M., Phung, E., Costner, P. J., . . . Team, V. R. C. S. (2019). A proof of concept for structure-based vaccine design targeting RSV in humans. *Science, 365*(6452), 505-509. doi:10.1126/science.aav9033

Davidson, E., & Doranz, B. J. (2014). A high-throughput shotgun mutagenesis approach to mapping B-cell antibody epitopes. *Immunology, 143*(1), 13-20. doi:10.1111/imm.12323

Davis, C. W., Jackson, K. J. L., McElroy, A. K., Halfmann, P., Huang, J., Chennareddy, C., . . . Ahmed, R. (2019). Longitudinal Analysis of the Human B Cell Response to Ebola Virus Infection. *Cell, 177*(6), 1566-1582 e1517. doi:10.1016/j.cell.2019.04.036

Davis, C. W., Nguyen, H. Y., Hanna, S. L., Sanchez, M. D., Doms, R. W., & Pierson, T. C. (2006). West Nile virus discriminates between DC-SIGN and DC-SIGNR for cellular attachment and infection. *J Virol, 80*(3), 1290-1301. doi:10.1128/JVI.80.3.1290-1301.2006

de Alwis, R., Smith, S. A., Olivarez, N. P., Messer, W. B., Huynh, J. P., Wahala, W. M., . . . de Silva, A. M. (2012). Identification of human neutralizing antibodies that bind to complex epitopes on dengue virions. *Proc Natl Acad Sci U S A, 109*(19), 7439-7444. doi:10.1073/pnas.1200566109

Dejnirattisai, W., Wongwiwat, W., Supasa, S., Zhang, X., Dai, X., Rouvinski, A., . . . Screaton, G. R. (2015). A new class of highly potent, broadly neutralizing antibodies isolated from

viremic patients infected with dengue virus. *Nat Immunol, 16*(2), 170-177. doi:10.1038/ni.3058

Deng, Y. Q., Dai, J. X., Ji, G. H., Jiang, T., Wang, H. J., Yang, H. O., . . . Qin, C. F. (2011). A broadly flavivirus cross-neutralizing monoclonal antibody that recognizes a novel epitope within the fusion loop of E protein. *PLoS One, 6*(1), e16059. doi:10.1371/journal.pone.0016059

Doria-Rose, N. A., Louder, M. K., Yang, Z., O'Dell, S., Nason, M., Schmidt, S. D., . . . Mascola, J. R. (2012). HIV-1 neutralization coverage is improved by combining monoclonal antibodies that target independent epitopes. *J Virol, 86*(6), 3393-3397. doi:10.1128/JVI.06745-11

Dowd, K. A., DeMaso, C. R., Pelc, R. S., Speer, S. D., Smith, A. R. Y., Goo, L., . . . Pierson, T. C. (2016). Broadly Neutralizing Activity of Zika Virus-Immune Sera Identifies a Single Viral Serotype. *Cell Rep, 16*(6), 1485-1491. doi:10.1016/j.celrep.2016.07.049

Dowd, K. A., Jost, C. A., Durbin, A. P., Whitehead, S. S., & Pierson, T. C. (2011). A dynamic landscape for antibody binding modulates antibody-mediated neutralization of West Nile virus. *PLoS Pathog, 7*(6), e1002111. doi:10.1371/journal.ppat.1002111

Fibriansah, G., Tan, J. L., Smith, S. A., de Alwis, A. R., Ng, T. S., Kostyuchenko, V. A., . . . Lok, S. M. (2014). A potent anti-dengue human antibody preferentially recognizes the conformation of E protein monomers assembled on the virus surface. *EMBO Mol Med, 6*(3), 358-371. doi:10.1002/emmm.201303404

Goo, L., Debbink, K., Kose, N., Sapparapu, G., Doyle, M. P., Wessel, A. W., . . . Pierson, T. C. (2019). A protective human monoclonal antibody targeting the West Nile virus E protein preferentially recognizes mature virions. *Nat Microbiol, 4*(1), 71-77. doi:10.1038/s41564-018-0283-7

Goo, L., Jalalian-Lechak, Z., Richardson, B. A., & Overbaugh, J. (2012). A combination of broadly neutralizing HIV-1 monoclonal antibodies targeting distinct epitopes effectively neutralizes variants found in early infection. *J Virol, 86*(19), 10857-10861. doi:10.1128/JVI.01414-12

Goo, L., VanBlargan, L. A., Dowd, K. A., Diamond, M. S., & Pierson, T. C. (2017). A single mutation in the envelope protein modulates flavivirus antigenicity, stability, and pathogenesis. *PLoS Pathog, 13*(2), e1006178. doi:10.1371/journal.ppat.1006178

Graham, B. S., Gilman, M. S. A., & McLellan, J. S. (2019). Structure-Based Vaccine Antigen Design. *Annu Rev Med, 70*, 91-104. doi:10.1146/annurev-med-121217-094234

Guzman, M. G., & Harris, E. (2015). Dengue. *Lancet, 385*(9966), 453-465. doi:10.1016/S0140-6736(14)60572-9

Hadinegoro, S. R., Arredondo-Garcia, J. L., Capeding, M. R., Deseda, C., Chotpitayasunondh, T., Dietze, R., . . . Group, C.-T. D. V. W. (2015). Efficacy and Long-Term Safety of a Dengue Vaccine in Regions of Endemic Disease. *N Engl J Med, 373*(13), 1195-1206. doi:10.1056/NEJMoa1506223

Halstead, S. B. (2014). Dengue Antibody-Dependent Enhancement: Knowns and Unknowns. *Microbiol Spectr, 2*(6). doi:10.1128/microbiolspec.AID-0022-2014

Hasan, S. S., Miller, A., Sapparapu, G., Fernandez, E., Klose, T., Long, F., . . . Rossmann, M. G. (2017). A human antibody against Zika virus crosslinks the E protein to prevent infection. *Nat Commun, 8*, 14722. doi:10.1038/ncomms14722

Hoehn, K. B., Fowler, A., Lunter, G., & Pybus, O. G. (2016). The Diversity and Molecular Evolution of B-Cell Receptors during Infection. *Mol Biol Evol, 33*(5), 1147-1157. doi:10.1093/molbev/msw015

Hu, D., Zhu, Z., Li, S., Deng, Y., Wu, Y., Zhang, N., . . . Ying, T. (2019). A broadly neutralizing germline-like human monoclonal antibody against dengue virus envelope domain III. *PLoS Pathog, 15*(6), e1007836. doi:10.1371/journal.ppat.1007836

Juraska, M., Magaret, C. A., Shao, J., Carpp, L. N., Fiore-Gartland, A. J., Benkeser, D., . . . Gilbert, P. B. (2018). Viral genetic diversity and protective efficacy of a tetravalent dengue vaccine in two phase 3 trials. *Proc Natl Acad Sci U S A, 115*(36), E8378-E8387. doi:10.1073/pnas.1714250115

Katzelnick, L. C., Fonville, J. M., Gromowski, G. D., Bustos Arriaga, J., Green, A., James, S. L., . . . Smith, D. J. (2015). Dengue viruses cluster antigenically but not as discrete serotypes. *Science, 349*(6254), 1338-1343. doi:10.1126/science.aac5017

Katzelnick, L. C., Gresh, L., Halloran, M. E., Mercado, J. C., Kuan, G., Gordon, A., . . . Harris, E. (2017). Antibody-dependent enhancement of severe dengue disease in humans. *Science, 358*(6365), 929-932. doi:10.1126/science.aan6836

Kaufmann, B., Vogt, M. R., Goudsmit, J., Holdaway, H. A., Aksyuk, A. A., Chipman, P. R., . . . Rossmann, M. G. (2010). Neutralization of West Nile virus by cross-linking of its surface proteins with Fab fragments of the human monoclonal antibody CR4354. *Proc Natl Acad Sci U S A, 107*(44), 18950-18955. doi:10.1073/pnas.1011036107

Keeffe, J. R., Van Rompay, K. K. A., Olsen, P. C., Wang, Q., Gazumyan, A., Azzopardi, S. A., . . . Robbiani, D. F. (2018). A Combination of Two Human Monoclonal Antibodies Prevents Zika Virus Escape Mutations in Non-human Primates. *Cell Rep, 25*(6), 1385-1394 e1387. doi:10.1016/j.celrep.2018.10.031

Khursheed, M., Khan, U. R., Ejaz, K., Fayyaz, J., Qamar, I., & Razzak, J. A. (2013). A comparison of WHO guidelines issued in 1997 and 2009 for dengue fever - single centre experience. *J Pak Med Assoc, 63*(6), 670-674. Retrieved from https://www.ncbi.nlm.nih.gov/pubmed/23901662

Kong, R., Louder, M. K., Wagh, K., Bailer, R. T., deCamp, A., Greene, K., . . . Mascola, J. R. (2015). Improving neutralization potency and breadth by combining broadly reactive HIV-1 antibodies targeting major neutralization epitopes. *J Virol, 89*(5), 2659-2671. doi:10.1128/JVI.03136-14

Kostyuchenko, V. A., Lim, E. X., Zhang, S., Fibriansah, G., Ng, T. S., Ooi, J. S., . . . Lok, S. M. (2016). Structure of the thermally stable Zika virus. *Nature, 533*(7603), 425-428. doi:10.1038/nature17994

Kraemer, M. U. G., Reiner, R. C., Jr., Brady, O. J., Messina, J. P., Gilbert, M., Pigott, D. M., . . . Golding, N. (2019). Past and future spread of the arbovirus vectors Aedes aegypti and Aedes albopictus. *Nat Microbiol, 4*(5), 854-863. doi:10.1038/s41564-019-0376-y

Kuhn, R. J., Zhang, W., Rossmann, M. G., Pletnev, S. V., Corver, J., Lenches, E., . . . Strauss, J. H. (2002). Structure of dengue virus: implications for flavivirus organization, maturation, and fusion. *Cell, 108*(5), 717-725. doi:10.1016/s0092-8674(02)00660-8

Kwong, P. D., & Mascola, J. R. (2018). HIV-1 Vaccines Based on Antibody Identification, B Cell Ontogeny, and Epitope Structure. *Immunity, 48*(5), 855-871. doi:10.1016/j.immuni.2018.04.029

Li, L., Meng, W., Horton, M., DiStefano, D. R., Thoryk, E. A., Pfaff, J. M., . . . Zhang, N. (2019). Potent neutralizing antibodies elicited by dengue vaccine in rhesus macaque target diverse epitopes. *PLoS Pathog, 15*(6), e1007716. doi:10.1371/journal.ppat.1007716

Lim, X. N., Shan, C., Marzinek, J. K., Dong, H., Ng, T. S., Ooi, J. S. G., . . . Lok, S. M. (2019). Molecular basis of dengue virus serotype 2 morphological switch from 29 degrees C to 37 degrees C. *PLoS Pathog, 15*(9), e1007996. doi:10.1371/journal.ppat.1007996

Lingwood, D., McTamney, P. M., Yassine, H. M., Whittle, J. R., Guo, X., Boyington, J. C., . . . Nabel, G. J. (2012). Structural and genetic basis for development of broadly neutralizing influenza antibodies. *Nature, 489*(7417), 566-570. doi:10.1038/nature11371

Littaua, R., Kurane, I., & Ennis, F. A. (1990). Human IgG Fc receptor II mediates antibody-dependent enhancement of dengue virus infection. *J Immunol, 144*(8), 3183-3186. Retrieved from https://www.ncbi.nlm.nih.gov/pubmed/2139079

Lok, S. M., Kostyuchenko, V., Nybakken, G. E., Holdaway, H. A., Battisti, A. J., Sukupolvi-Petty, S., . . . Rossmann, M. G. (2008). Binding of a neutralizing antibody to dengue virus alters the arrangement of surface glycoproteins. *Nat Struct Mol Biol, 15*(3), 312-317. doi:10.1038/nsmb.1382

MacLeod, D. T., Choi, N. M., Briney, B., Garces, F., Ver, L. S., Landais, E., . . . Poignard, P. (2016). Early Antibody Lineage Diversification and Independent Limb Maturation Lead to Broad HIV-1 Neutralization Targeting the Env High-Mannose Patch. *Immunity, 44*(5), 1215-1226. doi:10.1016/j.immuni.2016.04.016

Messina, J. P., Brady, O. J., Golding, N., Kraemer, M. U. G., Wint, G. R. W., Ray, S. E., . . . Hay, S. I. (2019). The current and future global distribution and population at risk of dengue. *Nat Microbiol, 4*(9), 1508-1515. doi:10.1038/s41564-019-0476-8

Messina, J. P., Brady, O. J., Scott, T. W., Zou, C., Pigott, D. M., Duda, K. A., . . . Hay, S. I. (2014). Global spread of dengue virus types: mapping the 70 year history. *Trends Microbiol, 22*(3), 138-146. doi:10.1016/j.tim.2013.12.011

Mukhopadhyay, S., Kim, B. S., Chipman, P. R., Rossmann, M. G., & Kuhn, R. J. (2003). Structure of West Nile virus. *Science, 302*(5643), 248. doi:10.1126/science.1089316

Nelson, S., Jost, C. A., Xu, Q., Ess, J., Martin, J. E., Oliphant, T., . . . Pierson, T. C. (2008). Maturation of West Nile virus modulates sensitivity to antibody-mediated neutralization. *PLoS Pathog, 4*(5), e1000060. doi:10.1371/journal.ppat.1000060

Nybakken, G. E., Oliphant, T., Johnson, S., Burke, S., Diamond, M. S., & Fremont, D. H. (2005). Structural basis of West Nile virus neutralization by a therapeutic antibody. *Nature, 437*(7059), 764-769. doi:10.1038/nature03956

Oliphant, T., Nybakken, G. E., Engle, M., Xu, Q., Nelson, C. A., Sukupolvi-Petty, S., . . . Diamond, M. S. (2006). Antibody recognition and neutralization determinants on domains I and II of West Nile Virus envelope protein. *J Virol, 80*(24), 12149-12159. doi:10.1128/JVI.01732-06

Paes, C., Ingalls, J., Kampani, K., Sulli, C., Kakkar, E., Murray, M., . . . Doranz, B. J. (2009). Atomic-level mapping of antibody epitopes on a GPCR. *J Am Chem Soc, 131*(20), 6952-6954. doi:10.1021/ja900186n

Parameswaran, P., Liu, Y., Roskin, K. M., Jackson, K. K., Dixit, V. P., Lee, J. Y., . . . Fire, A. Z. (2013). Convergent antibody signatures in human dengue. *Cell Host Microbe, 13*(6), 691-700. doi:10.1016/j.chom.2013.05.008

Patel, B., Longo, P., Miley, M. J., Montoya, M., Harris, E., & de Silva, A. M. (2017). Dissecting the human serum antibody response to secondary dengue virus infections. *PLoS Negl Trop Dis, 11*(5), e0005554. doi:10.1371/journal.pntd.0005554

Pierson, T. C., & Diamond, M. S. (2012). Degrees of maturity: the complex structure and biology of flaviviruses. *Curr Opin Virol, 2*(2), 168-175. doi:10.1016/j.coviro.2012.02.011

Pierson, T. C., Sanchez, M. D., Puffer, B. A., Ahmed, A. A., Geiss, B. J., Valentine, L. E., . . . Doms, R. W. (2006). A rapid and quantitative assay for measuring antibody-mediated neutralization of West Nile virus infection. *Virology, 346*(1), 53-65. doi:10.1016/j.virol.2005.10.030

Pierson, T. C., Xu, Q., Nelson, S., Oliphant, T., Nybakken, G. E., Fremont, D. H., & Diamond, M. S. (2007). The stoichiometry of antibody-mediated neutralization and enhancement of West Nile virus infection. *Cell Host Microbe, 1*(2), 135-145. doi:10.1016/j.chom.2007.03.002

Prasad, V. M., Miller, A. S., Klose, T., Sirohi, D., Buda, G., Jiang, W., . . . Rossmann, M. G. (2017). Structure of the immature Zika virus at 9 A resolution. *Nat Struct Mol Biol, 24*(2), 184-186. doi:10.1038/nsmb.3352

Priyamvada, L., Cho, A., Onlamoon, N., Zheng, N. Y., Huang, M., Kovalenkov, Y., . . . Wrammert, J. (2016). B Cell Responses during Secondary Dengue Virus Infection Are

Dominated by Highly Cross-Reactive, Memory-Derived Plasmablasts. *J Virol, 90*(12), 5574-5585. doi:10.1128/JVI.03203-15

Raut, R., Corbett, K. S., Tennekoon, R. N., Premawansa, S., Wijewickrama, A., Premawansa, G., . . . de Silva, A. M. (2019). Dengue type 1 viruses circulating in humans are highly infectious and poorly neutralized by human antibodies. *Proc Natl Acad Sci U S A, 116*(1), 227-232. doi:10.1073/pnas.1812055115

Robbiani, D. F., Bozzacco, L., Keeffe, J. R., Khouri, R., Olsen, P. C., Gazumyan, A., . . . Nussenzweig, M. C. (2017). Recurrent Potent Human Neutralizing Antibodies to Zika Virus in Brazil and Mexico. *Cell, 169*(4), 597-609 e511. doi:10.1016/j.cell.2017.04.024

Rogers, T. F., Goodwin, E. C., Briney, B., Sok, D., Beutler, N., Strubel, A., . . . Walker, L. M. (2017). Zika virus activates de novo and cross-reactive memory B cell responses in dengue-experienced donors. *Sci Immunol, 2*(14). doi:10.1126/sciimmunol.aan6809

Rouvinski, A., Guardado-Calvo, P., Barba-Spaeth, G., Duquerroy, S., Vaney, M. C., Kikuti, C. M., . . . Rey, F. A. (2015). Recognition determinants of broadly neutralizing human antibodies against dengue viruses. *Nature, 520*(7545), 109-113. doi:10.1038/nature14130

Salje, H., Cummings, D. A. T., Rodriguez-Barraquer, I., Katzelnick, L. C., Lessler, J., Klungthong, C., . . . Cauchemez, S. (2018). Reconstruction of antibody dynamics and infection histories to evaluate dengue risk. *Nature, 557*(7707), 719-723. doi:10.1038/s41586-018-0157-4

Sangkawibha, N., Rojanasuphot, S., Ahandrik, S., Viriyapongse, S., Jatanasen, S., Salitul, V., . . . Halstead, S. B. (1984). Risk factors in dengue shock syndrome: a prospective epidemiologic study in Rayong, Thailand. I. The 1980 outbreak. *Am J Epidemiol, 120*(5), 653-669. doi:10.1093/oxfordjournals.aje.a113932

Scheid, J. F., Mouquet, H., Feldhahn, N., Walker, B. D., Pereyra, F., Cutrell, E., . . . Nussenzweig, M. C. (2009). A method for identification of HIV gp140 binding memory B cells in human blood. *J Immunol Methods, 343*(2), 65-67. doi:10.1016/j.jim.2008.11.012

Scheid, J. F., Mouquet, H., Ueberheide, B., Diskin, R., Klein, F., Oliveira, T. Y., . . . Nussenzweig, M. C. (2011). Sequence and structural convergence of broad and potent HIV antibodies that mimic CD4 binding. *Science, 333*(6049), 1633-1637. doi:10.1126/science.1207227

Scherwitzl, I., Mongkolsapaja, J., & Screaton, G. (2017). Recent advances in human flavivirus vaccines. *Curr Opin Virol, 23*, 95-101. doi:10.1016/j.coviro.2017.04.002

Shen, W. F., Galula, J. U., Liu, J. H., Liao, M. Y., Huang, C. H., Wang, Y. C., . . . Chao, D. Y. (2018). Epitope resurfacing on dengue virus-like particle vaccine preparation to induce broad neutralizing antibody. *Elife, 7*. doi:10.7554/eLife.38970

Shi, X., Deng, Y., Wang, H., Ji, G., Tan, W., Jiang, T., . . . Guo, Y. (2016). A bispecific antibody effectively neutralizes all four serotypes of dengue virus by simultaneous blocking virus attachment and fusion. *MAbs, 8*(3), 574-584. doi:10.1080/19420862.2016.1148850

Sirohi, D., Chen, Z., Sun, L., Klose, T., Pierson, T. C., Rossmann, M. G., & Kuhn, R. J. (2016). The 3.8 A resolution cryo-EM structure of Zika virus. *Science, 352*(6284), 467-470. doi:10.1126/science.aaf5316

Smith, S. A., de Alwis, A. R., Kose, N., Harris, E., Ibarra, K. D., Kahle, K. M., . . . Crowe, J. E., Jr. (2013). The potent and broadly neutralizing human dengue virus-specific monoclonal antibody 1C19 reveals a unique cross-reactive epitope on the bc loop of domain II of the envelope protein. *MBio, 4*(6), e00873-00813. doi:10.1128/mBio.00873-13

Stiasny, K., Kiermayr, S., Holzmann, H., & Heinz, F. X. (2006). Cryptic properties of a cluster of dominant flavivirus cross-reactive antigenic sites. *J Virol, 80*(19), 9557-9568. doi:10.1128/JVI.00080-06

Sukupolvi-Petty, S., Austin, S. K., Engle, M., Brien, J. D., Dowd, K. A., Williams, K. L., . . . Diamond, M. S. (2010). Structure and function analysis of therapeutic monoclonal

antibodies against dengue virus type 2. *J Virol, 84*(18), 9227-9239. doi:10.1128/JVI.01087-10

Sukupolvi-Petty, S., Brien, J. D., Austin, S. K., Shrestha, B., Swayne, S., Kahle, K., . . . Diamond, M. S. (2013). Functional analysis of antibodies against dengue virus type 4 reveals strain-dependent epitope exposure that impacts neutralization and protection. *J Virol, 87*(16), 8826-8842. doi:10.1128/JVI.01314-13

Teoh, E. P., Kukkaro, P., Teo, E. W., Lim, A. P., Tan, T. T., Yip, A., . . . MacAry, P. A. (2012). The structural basis for serotype-specific neutralization of dengue virus by a human antibody. *Sci Transl Med, 4*(139), 139ra183. doi:10.1126/scitranslmed.3003888

Tharakaraman, K., Robinson, L. N., Hatas, A., Chen, Y. L., Siyue, L., Raguram, S., . . . Sasisekharan, R. (2013). Redesign of a cross-reactive antibody to dengue virus with broad-spectrum activity and increased in vivo potency. *Proc Natl Acad Sci U S A, 110*(17), E1555-1564. doi:10.1073/pnas.1303645110

Thein, T. L., Leo, Y. S., Lee, V. J., Sun, Y., & Lye, D. C. (2011). Validation of probability equation and decision tree in predicting subsequent dengue hemorrhagic fever in adult dengue inpatients in Singapore. *Am J Trop Med Hyg, 85*(5), 942-945. doi:10.4269/ajtmh.2011.11-0149

Tsai, W. Y., Durbin, A., Tsai, J. J., Hsieh, S. C., Whitehead, S., & Wang, W. K. (2015). Complexity of Neutralizing Antibodies against Multiple Dengue Virus Serotypes after Heterotypic Immunization and Secondary Infection Revealed by In-Depth Analysis of Cross-Reactive Antibodies. *J Virol, 89*(14), 7348-7362. doi:10.1128/JVI.00273-15

Tsai, W. Y., Lai, C. Y., Wu, Y. C., Lin, H. E., Edwards, C., Jumnainsong, A., . . . Wang, W. K. (2013). High-avidity and potently neutralizing cross-reactive human monoclonal antibodies derived from secondary dengue virus infection. *J Virol, 87*(23), 12562-12575. doi:10.1128/JVI.00871-13

Tzarum, N., Giang, E., Kong, L., He, L., Prentoe, J., Augestad, E., . . . Law, M. (2019). Genetic and structural insights into broad neutralization of hepatitis C virus by human VH1-69 antibodies. *Sci Adv, 5*(1), eaav1882. doi:10.1126/sciadv.aav1882

Vogt, M. R., Moesker, B., Goudsmit, J., Jongeneelen, M., Austin, S. K., Oliphant, T., . . . Diamond, M. S. (2009). Human monoclonal antibodies against West Nile virus induced by natural infection neutralize at a postattachment step. *J Virol, 83*(13), 6494-6507. doi:10.1128/JVI.00286-09

Walker, L. M., Phogat, S. K., Chan-Hui, P. Y., Wagner, D., Phung, P., Goss, J. L., . . . Burton, D. R. (2009). Broad and potent neutralizing antibodies from an African donor reveal a new HIV-1 vaccine target. *Science, 326*(5950), 285-289. doi:10.1126/science.1178746

Waltari, E., McGeever, A., Friedland, N., Kim, P. S., & McCutcheon, K. M. (2019). Functional Enrichment and Analysis of Antigen-Specific Memory B Cell Antibody Repertoires in PBMCs. *Front Immunol, 10*, 1452. doi:10.3389/fimmu.2019.01452

Woda, M., & Mathew, A. (2015). Fluorescently labeled dengue viruses as probes to identify antigen-specific memory B cells by multiparametric flow cytometry. *J Immunol Methods, 416*, 167-177. doi:10.1016/j.jim.2014.12.001

Wrammert, J., Onlamoon, N., Akondy, R. S., Perng, G. C., Polsrila, K., Chandele, A., . . . Ahmed, R. (2012). Rapid and massive virus-specific plasmablast responses during acute dengue virus infection in humans. *J Virol, 86*(6), 2911-2918. doi:10.1128/JVI.06075-11

Wu, X., Yang, Z. Y., Li, Y., Hogerkorp, C. M., Schief, W. R., Seaman, M. S., . . . Mascola, J. R. (2010). Rational design of envelope identifies broadly neutralizing human monoclonal antibodies to HIV-1. *Science, 329*(5993), 856-861. doi:10.1126/science.1187659

Wu, X., Zhou, T., Zhu, J., Zhang, B., Georgiev, I., Wang, C., . . . Mascola, J. R. (2011). Focused evolution of HIV-1 neutralizing antibodies revealed by structures and deep sequencing. *Science, 333*(6049), 1593-1602. doi:10.1126/science.1207532

Xu, M., Hadinoto, V., Appanna, R., Joensson, K., Toh, Y. X., Balakrishnan, T., . . . Fink, K. (2012). Plasmablasts generated during repeated dengue infection are virus glycoprotein-specific and bind to multiple virus serotypes. *J Immunol, 189*(12), 5877-5885. doi:10.4049/jimmunol.1201688

Xu, M., Zuest, R., Velumani, S., Tukijan, F., Toh, Y. X., Appanna, R., . . . Fink, K. (2017). A potent neutralizing antibody with therapeutic potential against all four serotypes of dengue virus. *NPJ Vaccines, 2*, 2. doi:10.1038/s41541-016-0003-3

Xu, M., Zust, R., Toh, Y. X., Pfaff, J. M., Kahle, K. M., Davidson, E., . . . Fink, K. (2016). Protective Capacity of the Human Anamnestic Antibody Response during Acute Dengue Virus Infection. *J Virol, 90*(24), 11122-11131. doi:10.1128/JVI.01096-16

Yu, I. M., Zhang, W., Holdaway, H. A., Li, L., Kostyuchenko, V. A., Chipman, P. R., . . . Chen, J. (2008). Structure of the immature dengue virus at low pH primes proteolytic maturation. *Science, 319*(5871), 1834-1837. doi:10.1126/science.1153264

Zanini, F., Robinson, M. L., Croote, D., Sahoo, M. K., Sanz, A. M., Ortiz-Lasso, E., . . . Einav, S. (2018). Virus-inclusive single-cell RNA sequencing reveals the molecular signature of progression to severe dengue. *Proc Natl Acad Sci U S A, 115*(52), E12363-E12369. doi:10.1073/pnas.1813819115

Zhang, X., Ge, P., Yu, X., Brannan, J. M., Bi, G., Zhang, Q., . . . Zhou, Z. H. (2013). Cryo-EM structure of the mature dengue virus at 3.5-A resolution. *Nat Struct Mol Biol, 20*(1), 105-110. doi:10.1038/nsmb.2463

Zhang, Y., Corver, J., Chipman, P. R., Zhang, W., Pletnev, S. V., Sedlak, D., . . . Rossmann, M. G. (2003). Structures of immature flavivirus particles. *EMBO J, 22*(11), 2604-2613. doi:10.1093/emboj/cdg270

Zhang, Y., Kaufmann, B., Chipman, P. R., Kuhn, R. J., & Rossmann, M. G. (2007). Structure of immature West Nile virus. *J Virol, 81*(11), 6141-6145. doi:10.1128/JVI.00037-07

Zhou, J. Q., & Kleinstein, S. H. (2019). Cutting Edge: Ig H Chains Are Sufficient to Determine Most B Cell Clonal Relationships. *J Immunol, 203*(7), 1687-1692. doi:10.4049/jimmunol.1900666

Figure 1

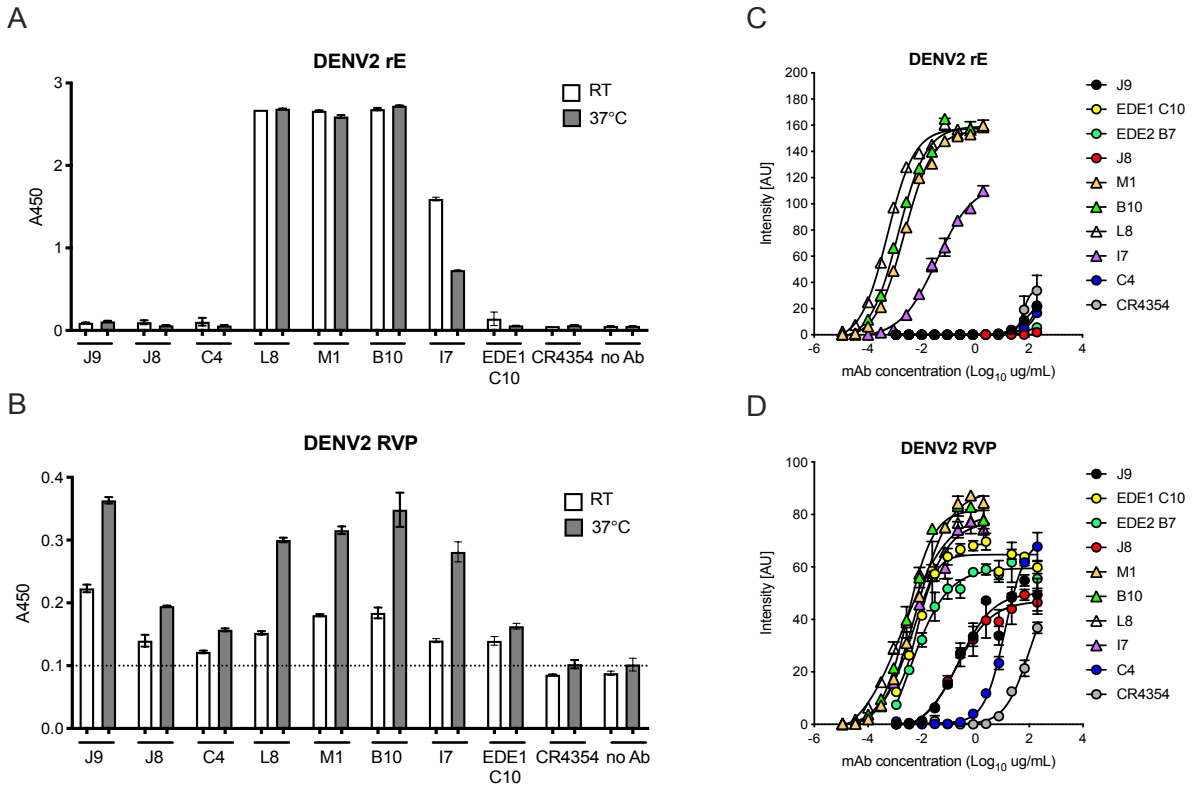

*

*

Figure 2

A

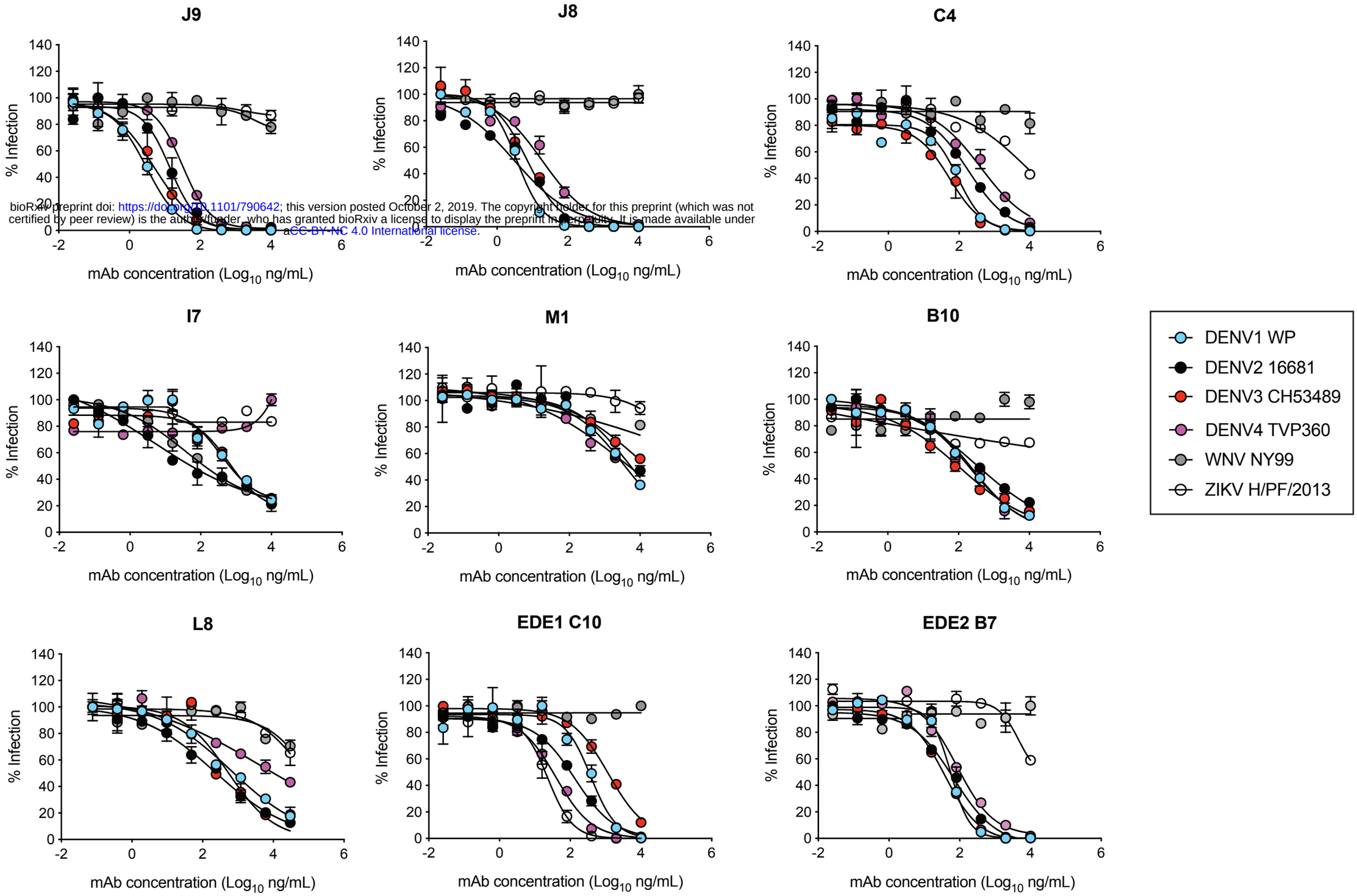

B

	Shared clonal family				Shared clonal family					
	Pt 013	Pt 013	Pt 013	Pt 013	Pt 013	Pt 020	Pt 020			
	J9	J8	C4	I7	M1	B10	L8	EDE1 C10	EDE2 B7	CR4354
DENV1	6	9	69	1751	1091	757	360	352	91	
DENV2	30	18	262	1142	937	929	177	171	64	
DENV3	15	13	36	1771	2156	499	292	753	45	
DENV4	39	70	1624		900	698	2454	38	206	
ZIKV								38		
WNV				620						7

IC_{50} (ng/mL)
<10
10-100
101-1000
1001-10000
>10000

Figure 3

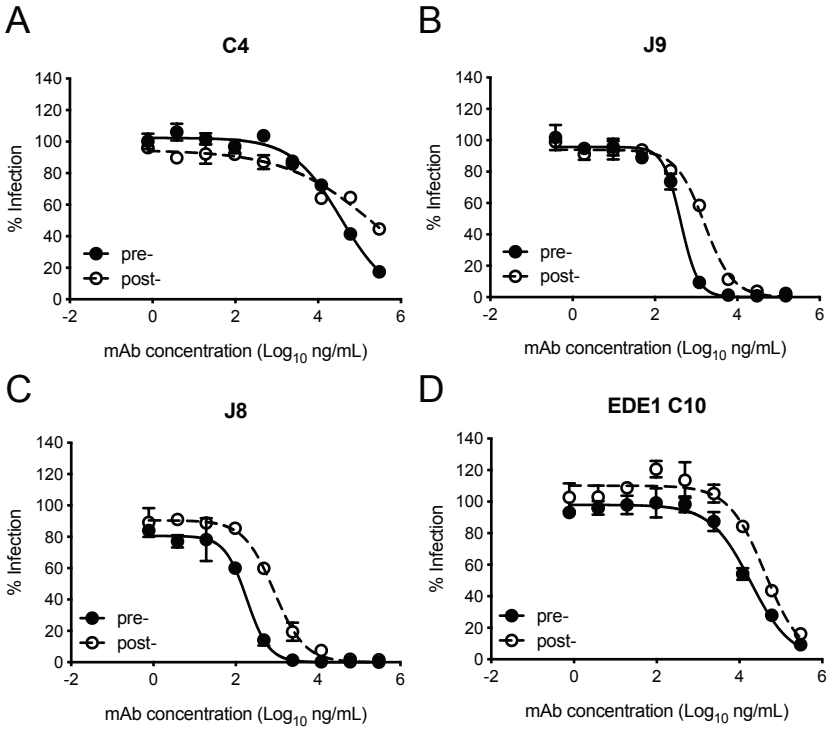
A
C4
B
J9
C
J8
D
EDE1 C10
% Infection
mAb concentration (Log10 ng/mL)
pre-
post-
0
20
40
60
80
100
120
140
-2
0
2
4
6

Figure 4

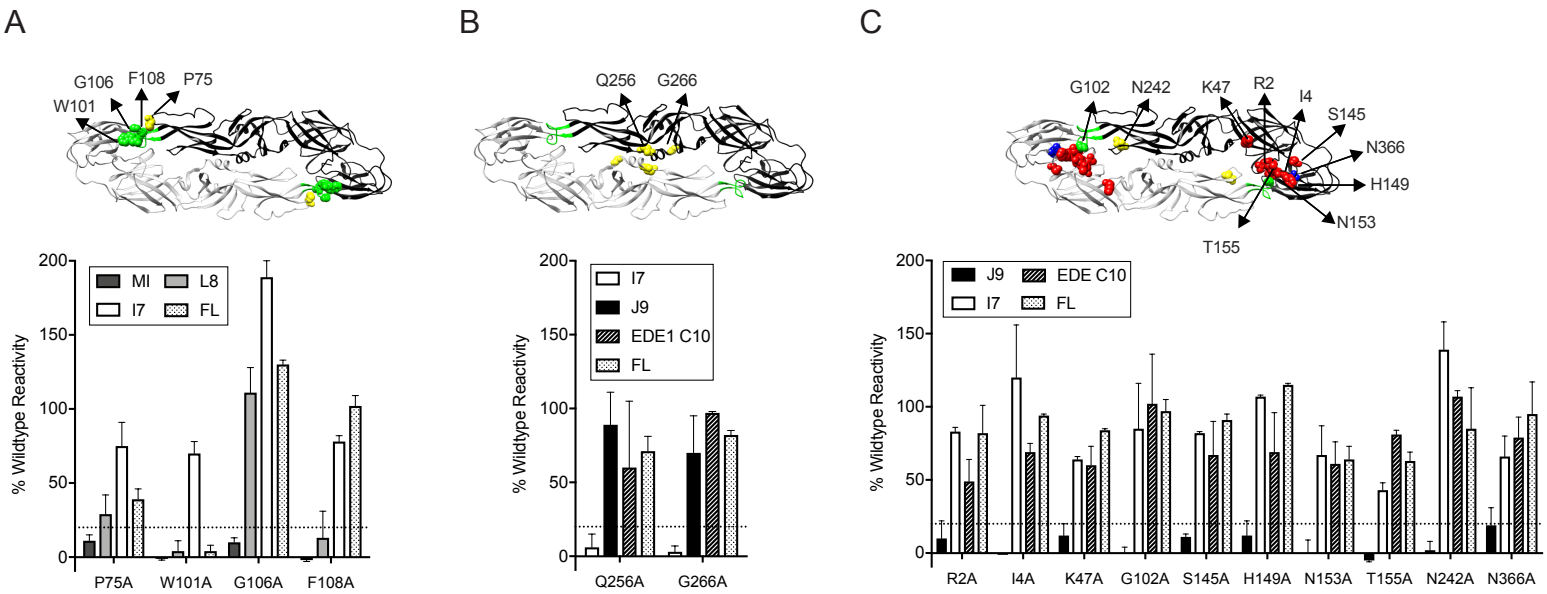

Figure 5

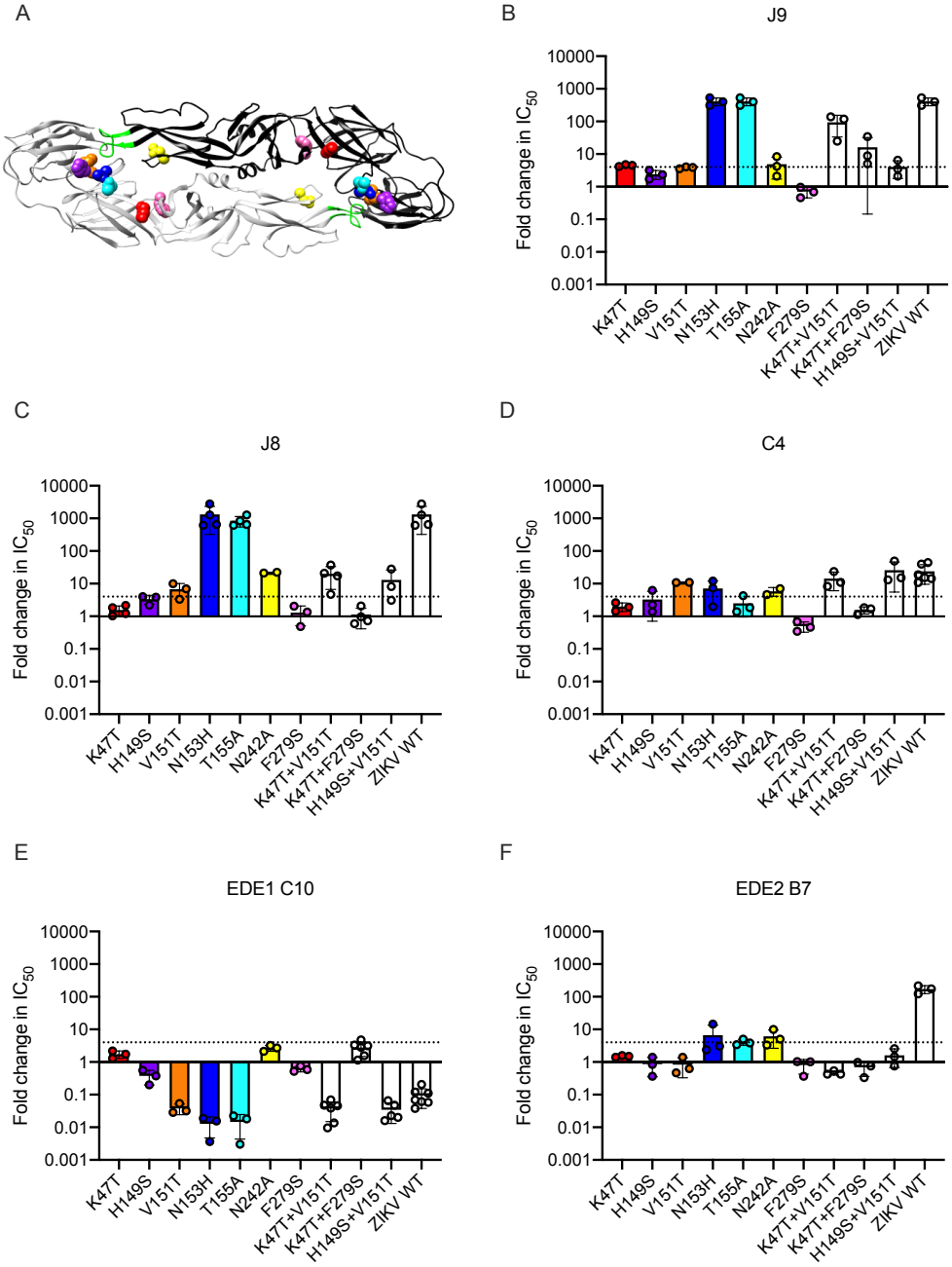

Figure 6

A

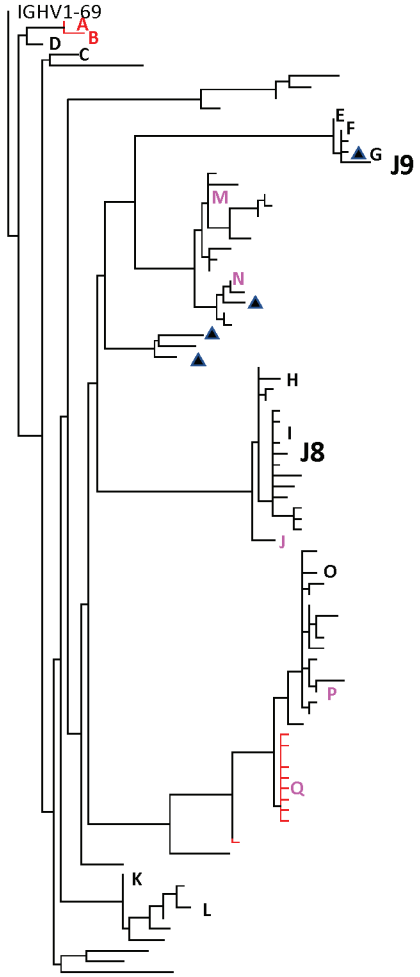

B

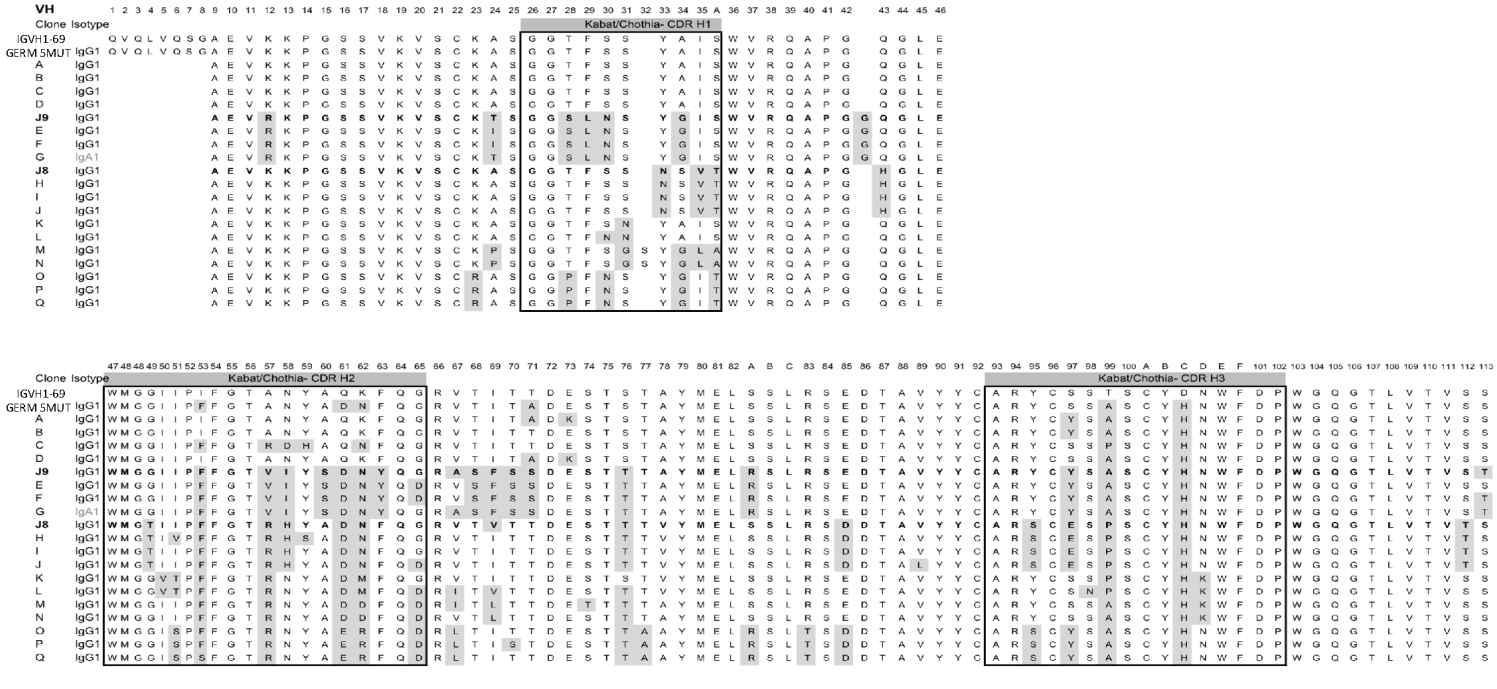

C

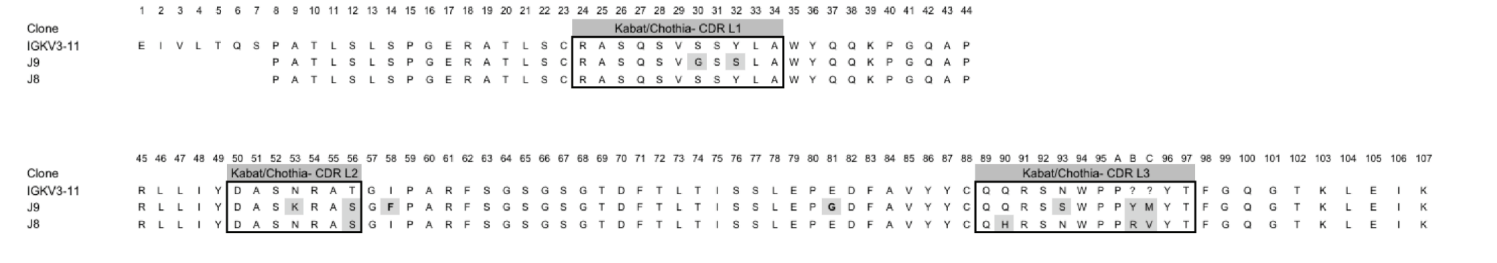

Figure 7

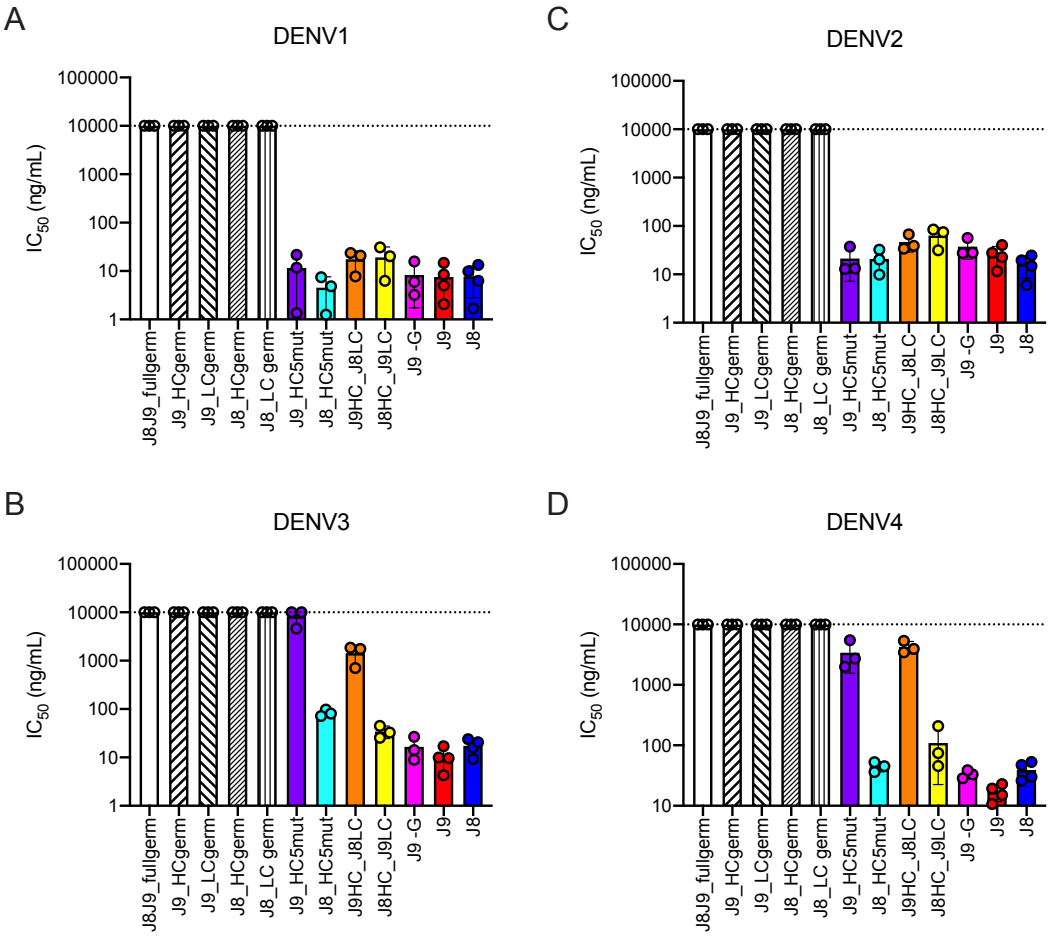

Table S1. Percent mAb binding reactivity to DENV2 E protein alanine scanning mutagenesis library normalized to wildtype DENV2

	J9		I7		M1		L8		EDE1 C10		FL	
Mutation	Mean	Range	Mean	Range	Mean	Range	Mean	Range	Mean	Range	Mean	Range
M1A	-2	4	83	3	48	2	44	6	4	2	87	0
R2A	10	12	83	3	49	8	54	6	49	15	82	19
C3A	5	16	37	17	30	3	24	7	-4	2	49	7
I4A	-1	0	120	36	77	15	67	15	69	6	94	1
G5A	-3	2	91	3	49	9	46	14	-2	5	87	3
M6A	89	17	121	39	98	3	96	8	82	10	126	29
S7A	82	46	127	18	78	9	77	15	106	3	111	7
N8A	79	12	60	0	76	13	60	4	99	19	81	14
R9A	2	13	52	7	36	3	39	8	-1	1	70	8
D10A	97	45	132	2	88	28	100	8	119	27	116	4
F11A	14	24	76	77					-3	17	51	10
V12A	75	10	90	62					118	5	76	9
E13A	63	38	79	22	75	5	74	4	90	16	83	6
G14A	87	44	164	37	86	5	102	3	92	19	86	16
V15A	90	23	100	14	86	17	94	2	141	18	111	13
S16A	101	9	149	76	93	27	89	20	135	51	104	6
G17A	91	3	132	77	81	7	76	24	130	29	98	22
G18A	131	29	126	24	94	1	120	23	120	34	116	7
S19A	113	39	117	45	87	11	85	29	108	62	97	17
W20A	119	45	83	23	66	7	63	19	77	25	99	19
V21A	59	4	49	3	66	17	65	4	93	23	81	10
D22A	17	7	14	13	23	2	28	4	34	33	32	2
I23A	15	4	5	7	8	5	13	4	7	4	26	1
V24A	66	22	93	0	76	9	80	21	87	41	86	2
L25A	6	8	-5	5	2	3	2	1	1	1	13	1
E26A	74	18	96	24	80	3	80	6	116	23	95	5
H27A	44	9	73	10	72	23	80	22	80	3	93	10
G28A	34	1	53	50					68	21	50	6
S29A	130	6	137	9	77	26	88	16	79	17	108	18
C30A	2	5	27	14	21	8	23	4	-1	5	43	5
V31A	47	1	27	7	30	15	37	9	52	14	51	6
T32A	4	7	6	1	7	5	7	0	-1	5	21	3
T33A	118	16	116	15	93	9	95	3	98	57	112	23
M34A	2	2	34	5	30	6	34	12	3	3	66	6
A35S	88	22	122	13	71	22	69	8	66	6	99	10
K36A	120	29	115	18	83	20	83	1	69	1	106	5
N37A	68	11	68	14	50	10	56	6	67	14	78	6
K38A	54	6	71	28	55	15	61	1	75	12	77	4
P39A	2	1	27	7	19	3	22	4	4	3	41	3
T40A	-1	0	55	11	37	2	34	1	4	6	62	4
L41A	-3	0	2	1	2	1	5	2	-4	1	15	2
D42A	5	6	19	0	19	7	19	1	0	2	43	0
F43A	25	5	6	10	16	9	19	6	22	0	25	2

E44A	81	4	118	5	87	9	81	5	72	41	102	7
L45A	-2	3	-5	10	0	2	1	0	0	4	6	1
I46A	19	8	25	3	33	7	30	10	44	0	57	7
K47A	12	8	64	2	57	20	61	1	60	13	84	1
T48A	55	7	91	21	80	36	81	1	68	16	89	9
E49A	74	11	68	33	62	16	62	15	85	17	79	4
A50S	55	6	74	44	60	23	60	17	55	15	83	1
K51A	46	20	45	17	60	11	54	10	58	0	74	3
Q52A	108	27	99	41	82	16	107	16	114	63	106	7
P53A	98	37	170	0	90	35	93	3	102	9	124	1
A54S	91	10	150	6	87	28	89	15	115	14	108	1
T55A	63	31	60	15	45	23	60	5	64	14	85	9
L56A	15	9	-4	5	6	3	5	1	14	4	25	1
R57A	7	1	-6	8	0	1	4	4	0	1	8	4
K58A	53	20	30	1	33	16	31	3	60	5	58	3
Y59A	-2	2	-5	7	0	2	2	2	-3	0	5	1
C60A	-3	0	-5	7	-1	2	1	1	2	4	2	1
I61A	3	7	-4	4	0	3	2	3	0	5	6	1
E62A	79	36	76	1	63	25	54	14	73	2	94	4
A63S	31	13	6	9	6	2	8	5	14	1	31	5
K64A	149	6	186	4	100	11	116	27	130	20	130	8
L65A	80	44	37	11	54	11	59	9	64	4	72	8
T66A	55	15	49	11	53	19	58	12	93	5	78	7
N67A	38	2	12	7	20	2	19	0	62	0	37	1
T68A	90	61	109	9	76	32	80	9	93	18	90	4
T69A	58	5	35	11	30	6	34	4	86	1	45	1
T70A	42	7	36	10	27	8	31	1	61	16	52	3
E71A	149	89	182	54	94	22	112	12	162	21	110	21
S72A	119	0	122	12	80	20	88	9	114	32	104	6
R73A	92	40	124	22	86	23	78	16	71	7	104	3
C74A	1	2	1	4	-2	1	0	0	4	9	0	0
P75A	11	2	75	16	11	4	29	13	4	4	39	7
T76A	132	45	138	10	116	11	104	11	147	42	118	3
Q77A	109	38	117	20	65	8	75	7	72	28	103	21
G78A	67	16	52	11	46	21	59	11	44	9	82	1
E79A	0	2	-2	9	0	5	0	0	-1	1	3	1
P80A	80	33	92	9	54	5	60	14	79	38	70	4
S81A	110	38	106	9	76	6	80	25	92	10	99	19
L82A	40	11	41	13	12	8	23	5	57	11	45	5
N83A	119	2	195	37	100	5	114	7	151	66	130	47
E84A	64	18	79	35	59	16	74	29	65	30	83	21
E85A	25	13	30	2	16	3	22	5	29	4	42	4
Q86A	71	8	90	21	104	8	91	19	72	59	109	8
D87A	-2	2	-2	0	-1	2	2	1	0	3	6	0
K88A	106	12	138	52	113	4	108	8	108	12	106	1
R89A	74	12	42	1	44	4	42	3	89	6	79	20
F90A	7	9	9	3	4	3	7	1	7	8	21	1
V91A	53	21	14	8	16	2	16	4	41	22	45	2

C92A	1	10	3	1	-2	2	0	0	-6	0	3	3
K93A	137	24	63	3	73	3	78	10	93	44	93	14
H94A	33	12	30	6	18	6	20	2	31	18	40	3
S95A	54	14	98	23	72	6	84	19	116	26	102	4
M96A	90	2	70	11	75	14	83	6	60	1	86	4
V97A	42	15	49	15	46	21	49	6	74	14	72	5
D98A	1	3	50	3	25	8	33	0	10	4	62	4
R99A	5	2	73	71					-7	9	58	7
G100A	2	1	73	58					5	23	36	8
W101A	-3	1	70	8	-1	1	4	7	-4	1	4	4
G102A	0	4	85	31	69	14	50	4	102	34	97	8
N103A	-3	3	24	4	2	2	8	3	-3	8	25	1
G104A	26	3	33	4	12	2	16	5	2	4	35	7
C105A	-1	7	6	5	0	1	1	1	-3	1	4	0
G106A	161	62	189	12	10	3	111	17	172	12	130	3
L107A	103	37	123	9	101	20	114	3	105	21	113	9
F108A	0	6	78	4	-2	1	13	18	-3	1	102	7
G109A	43	10	50	1	22	6	29	3	34	9	41	0
K110A	45	1	83	15	55	2	51	4	50	1	69	8
G111A	51	28	85	31	37	7	67	7	65	0	76	8
G112A	101	31	169	82	116	8	96	1	126	52	124	7
I113A	48	5	44	21	29	11	37	13	73	22	59	10
V114A	33	12	20	11	14	1	20	12	29	28	39	4
T115A	6	5	4	8	11	8	10	1	15	2	35	0
C116A	0	6	-2	10	0	2	1	3	-2	3	2	2
A117S	93	10	85	7	73	3	82	0	76	37	104	3
M118A	63	6	53	3	39	8	42	1	85	1	64	23
F119A	0	1	-7	6	1	2	0	1	-2	3	2	2
R120A	127	50	85	6					97	19	136	21
K123A	88	5	67	83					82	10	77	20
N124A	110	54	210	61	139	39	131	0	116	62	153	8
M125A	60	11	59	17	45	11	47	10	78	5	71	1
E126A	100	29	84	6					58	20	101	21
G127A	51	13	13	6	17	10	20	6	48	14	41	1
K128A	94	16	68	7	54	9	63	14	60	16	84	3
V129A	54	3	75	22	60	16	68	9	77	37	72	3
V130A	49	6	17	5	21	9	30	8	48	6	50	5
Q131A	110	9	113	26	96	3	88	4	139	86	132	16
P132A	113	37	118	20	74	14	84	15	87	15	98	11
E133A	89	14	69	11	79	3	74	32	92	37	106	2
N134A	101	61	68	7	59	2	65	16	85	40	97	4
L135A	48	30	25	2	25	11	24	12	19	4	52	5
E136A	81	24	37	6	48	19	51	20	39	8	57	2
Y137A	10	0	3	8	15	5	15	2	10	7	30	2
T138A	21	1	15	0	18	9	19	4	20	4	37	3
I139A	12	5	7	9	7	5	9	0	11	6	18	4
V140A	100	32	159	51	101	18	112	7	143	34	118	0
I141A	49	2	33	16	36	9	37	12	61	31	52	1

T142A	75	15	83	35	62	1	73	13	76	22	87	5
P143A	47	10	66	21	51	18	51	15	56	5	75	15
H144A	17	9	39	33					29	6	54	6
S145A	11	2	82	1	69	35	65	8	67	23	91	4
G146A	-3	1	59	9	51	7	44	8	19	3	83	0
E147A	115	36	125	5	84	12	81	15	108	10	113	5
E148A	86	25	132	51	75	18	77	2	88	4	98	16
H149A	12	10	107	1	84	47	74	6	69	27	115	1
A150S	121	39	125	15	101	23	89	2	129	25	107	7
V151A	5	1	96	5	61	7	56	13	43	1	96	2
G152A	-3	1	59	1	52	17	54	8	24	11	89	2
N153A	0	9	67	20	48	9	53	19	61	15	64	9
D154A	91	36	120	5	95	17	108	11	80	6	111	8
T155A	-5	1	43	5	53	11	50	7	81	3	63	6
G156A	98	63	99	7					79	2	112	3
K157A	140	1	106	7	83	5	93	8	116	31	113	6
H158A	55	2	86	4	71	3	69	4	136	12	106	7
G159A	54	18	150	7	79	2	94	4	80	18	105	17
K160A	131	9	162	2	103	18	106	2	67	3	130	8
E161A	96	35	85	3	85	28	80	1	136	14	106	7
I162A	35	17	22	18	26	13	30	8	51	8	49	4
K163A	45	37	38	20	36	13	48	3	65	6	58	3
I164A	6	1	3	11	4	3	7	3	1	3	18	2
T165A	62	11	56	2	47	21	47	11	51	8	73	5
P166A	136	83	177	15	94	16	106	29	116	31	129	13
Q167A	138	76	129	15	77	35	90	14	88	10	97	4
S168A	96	29	127	21	82	33	81	25	131	67	102	12
S169A	109	45	111	3					70	63	121	9
I170A	104	47	103	32	82	17	83	32	118	45	100	9
T171A	114	30	142	36	101	32	103	15	150	49	144	1
E172A	94	59	77	33	65	13	69	20	72	37	91	11
A173S	57	28	50	16	47	13	52	9	69	27	70	3
E174A	94	3	103	14	76	29	64	18	123	12	91	8
L175A	0	1	-3	7	2	2	5	3	-1	3	14	0
T176A	120	55	125	44	95	16	83	13	112	17	120	15
G177A	25	22	23	6	28	5	30	6	30	6	50	1
Y178A	12	1	9	7	16	3	15	5	24	5	35	5
G179A	20	1	23	12					6	7	33	0
T180A	116	22	82	9	70	17	83	15	68	33	99	4
V181A	71	44	32	22	50	13	55	3	61	9	59	2
T182A	117	26	119	36	82	33	92	27	120	7	119	10
M183A	36	19	32	3	39	12	45	6	83	10	54	5
E184A	88	26	102	29	81	15	63	23	109	16	84	9
C185A	6	7	-3	3	1	2	2	0	-4	0	6	1
S186A	63	17	109	2	74	17	83	22	109	46	104	4
P187A	91	46	121	33	97	24	87	21	134	8	101	4
R188A	86	21	111	56	94	27	99	26	112	38	112	12
T189A	74	23	136	22	95	17	91	19	111	36	111	3

G190A	78	0	123	6	87	34	98	20	129	5	120	0
L191A	103	5	91	30					77	5	81	16
D192A	44	1	37	12	35	5	40	14	43	15	67	8
F193A	67	0	54	6	52	10	56	23	91	26	75	20
N194A	93	5	97	36	91	31	80	15	108	22	93	1
E195A	88	45	61						39	7	65	15
M196A	100	24	76	35	57	25	55	14	51	36	91	11
V197A	20	22	7	1	11	5	16	1	19	4	44	5
L198A	67	21	123	40	134	26	121	12	174	54	141	12
L199A	73	16	76	4	44	7	48	15	72	2	76	14
Q200A	61	22	55	6	47	14	50	16	87	7	81	13
M201A	47	19	38	10	24	5	28	8	58	15	55	11
E202A	79	13	121	2	91	18	81	1	87	31	97	1
N203A	53	11	37	10	40	1	43	9	68	3	60	10
K204A	96	10	20	4	43	14	46	11	100	8	63	0
A205S	96	3	74	12					81	9	92	38
W206A	37	12	-3	6	15	5	19	5	46	17	34	12
L207A	93	52	98	11	76	15	74	23	86	44	100	17
V208A	37	15	22	26	32	14	27	7	35	1	45	2
H209A	91	5	90	35	79	16	77	12	96	18	96	10
R210A	42	3	39	4	31	7	28	6	26	3	52	9
Q211A	87	21	71	11	67	5	81	15	117	33	96	1
W212A	25	4	-2	2	27	6	35	11	58	4	48	7
F213A	16	2	1	9	8	3	9	3	24	1	30	5
L214A	58	3	4						44	9	22	6
D215A	34	66	30	17					64	12	62	13
L216A	-3	0	-1	16	-1	3	1	0	3	9	5	1
P217A	105	20	154	10	81	13	96	17	69	51	83	25
L218A	1	4	-1	3					-12	8	1	1
P219A	5	2	11	19	2	7	1	0	-2	4	13	1
W220A	7	2	-2	7	2	3	2	0	1	4	11	2
L221A	80	8	84	6	67	16	51	48	77	48	93	4
P222A	47	89	123	70					80	3	84	10
G223A	75	10	53	12	70	8	76	5	55	4	86	11
A224S	85	7	167	13	121	20	109	7	106	58	112	3
D225A	50	12	67	8	73	22	73	22	67	10	80	19
T226A	93	26	110	47					116	22	88	16
Q227A	90	59	94	2	90	27	94	20	92	61	107	6
G228A	94	16	84	6	87	12	82	14	94	41	99	6
S229A	84	75	113	10	95	37	95	19	77	28	138	21
N230A	118	65	80	9					98	18	80	1
W231A	-1	2	-1	1					-5	8	-1	2
I232A	81	163	86	49					82	38	86	34
Q233A	124	70	147	77					85	2	91	3
K234A	117	107	87	8					63	12	88	19
E235A	30	62	40	68					37	3	28	1
T236A	96	31	96	22					73	19	90	53

L237A	89	36	51	100		39	23	31	5
V238A	24	48	31	51		51	3	38	10
T239A	63	127	127	74		59	55	114	26
F240A	34	70	45	71		29	21	20	3
K241A	55	104	96	56		73	14	95	21
N242A	2	6	139	19		85	28	107	4
P243A	97	13	111	84		84	26	74	18
H244A	68	12	82	11		80	8	60	2
A245S	97	3	88	4		104	20	80	16
K246A	56	22	98	39		108	27	118	46
K247A	104	35	118	1		106	11	89	17
Q248A	74	10	78	71		72	14	56	13
D249A	84	36	74	36		63	21	83	11
V250A	118	34	75	26		78	25	72	13
V251A	130	33	119	39		110	43	100	18
V252A	101	4	135	79		102	12	133	34
L253A	114	3	85	19		57	7	91	19
G254A	77	15	84	26		86	29	84	4
S255A	54	24	16	12		41	1	43	16
Q256A	89	22	6	9		60	45	71	10
E257A	101	19	74	3		73	6	73	14
G258A	54	17	92	38		55	0	90	19
A259S	93	22	61	2		60	7	69	2
M260A	18	7	46	84		6	11	15	8
H261A	109	28	77	32		60	1	82	16
T262A	61	97	98	49		141	3	108	37
A263S	69	51	51	56		64	0	62	14
L264A	40	1	-3	1		21	16	25	10
T265A	99	32	34	67		115	99	129	31
G266A	70	25	3	4		97	1	82	3
A267S	89	2	72	46		94	13	84	31
T268A	106	18	80	47		82	6	84	24
E269A	64	5	76	47		83	27	77	29
I270A	116	42	64	27		95	3	94	13
Q271A	98	70	75	22		130	22	92	27
M272A	73	17	65	21		146	18	97	29
S273A	112	10	99	18		87	27	100	32
S274A	103	13	74	5		85	19	97	16
G275A	135	20	66	35		90	0	57	8
N276A	128	7	76	28		108	17	96	51
L277A	56	46	97	10		111	90	127	11
L278A	44	35	126	55		92	19	96	11
F279A	28	15	76	31		86	78	70	19
T280A	52	31	113	37		130	19	127	19
G281A	8	0	83	100		43	36	48	20
H282A	104	15	128	54		142	4	130	32
L283A	36	18	52	48		46	1	69	23
K284A	77	4	80	5		58	33	84	21

C285A	3	8	37	80		30	58	4	2
R286A	68	30	47	56		54	2	37	1
L287A	124	8	59	2		102	8	98	12
R288A	73	27	62	17		94	14	60	29
M289A	23	1	18	13		12	4	29	3
D290A	64	1	50	30		49	18	53	14
K291A	56	28	80	29		71	1	65	19
L292A	19	20	50	31		25	1	50	20
Q293A	106	3	70	45		62	9	94	31
L294A	83	3	76	2		104	6	79	23
K295A	92	35	85	28		65	6	76	12
G296A	8	4	63	37		4	18	48	6
M297A	121	66	71	14		74	1	122	16
S298A	78	25	74	34		104	44	95	19
Y299A	60	10	72	39		54	5	62	10
S300A	91	45	108	77		111	4	93	25
M301A	89	24	103	62		115	17	94	28
C302A	3	2	41	84		-4	14	5	2
T303A	70	34	99	31		102	37	82	28
G304A	19	8	54	95		22	13	26	2
K305A	113	0	83	5		121	33	80	14
F306A	4	2	40	82		-6		8	3
K307A	86	1	76	24		104	16	72	31
V308A	31	42	93	87		53	52	78	11
V309A	47	89	52	7		57	10	75	29
K310A	7	1	68	41		-5	11	66	21
E311A	43	85	87	30		77	3	85	1
I312A	104	6	65	45		78	38	63	24
A313S	48	92	78	31		54	16	66	6
E314A	82	21	54	13		86	41	75	17
T315A	0	1	18			23	21	40	1
Q316A	27	55	152	92		40	9	71	18
H317A	25	48	85	33		100	38	80	18
G318A	41	30	58	33		48	7	59	5
T319A	-2	4	91	131		0	6	35	17
I320A	40	9	46	56		28	0	35	1
V321A	22	14	110	147		64	10	49	4
I322A	60	0	109	142		64	16	58	5
R323A	69	21	86	1		75	25	82	2
V324A	37	32	71	94		28	6	49	11
Q325A	133	55	103	0		91	11	102	14
Y326A	7	3	41	73		-3	6	12	2
E327A	127	48	78	2		88	19	76	22
G328A	55	17	65	55		35	4	56	18
D329A	153	81	121	35		79	23	99	3
G330A	104	27	78	39		59	3	90	9
S331A	141	21	114	32		85	33	122	6
P332A	36	4	30	30		10	0	33	3

C333A	2	1	10	11		3	3	5	3
K334A	68	18	69	25		49	4	63	14
I335A	9	0	34	66		16	13	12	0
P336A	52	35	88	106		31	8	50	10
F337A	62	7	64	74		35	8	38	13
E338A	136	32	107	12		114	36	105	1
I339A	10	5	47	90		-5	7	12	2
M340A	75	13	44	11		57	14	69	26
D341A	86	5	80	45		67	21	80	7
L342A	119	44	106	34		103	36	121	26
E343A	96	33	96	35		82	40	97	7
K344A	115	23	85	21		42	7	87	17
R345A	105	38	86	33		64	2	78	21
H346A	99	18	49	18		101	13	89	9
V347A	131	24	97	6		94	4	106	5
L348A	107	21	94	35		77	4	93	6
G349A	46	26	68	18		22	21	45	2
R350A	35	12	61	48		30	24	57	9
L351A	86	16	52	4		47	26	73	13
I352A	15	12	32	22		-5	17	39	8
T353A	29	12	25	33		12	1	38	11
V354A	104	61	143	44		77	42	119	27
N355A	104	31	83	19		53	23	78	20
P356A	25	3	68	36		41	22	54	14
I357A	45	5	67	23		29	5	66	14
V358A	58	63	127	99		103	34	55	7
T359A	99	37	71	8		113	7	91	34
E360A	97	24	107	41		101	76	111	31
K361A	94	6	81	38		107	39	92	32
D362A	96	12	77	34		94	0	113	30
S363A	112	26	143	91		97	16	101	27
P364A	95	13	116	63		97	5	96	39
V365A	56	9	51	42		43	3	53	2
N366A	19	12	66	14		79	14	95	22
I367A	7	3	1	3		2	6	8	3
E368A	5	1	47	70		-7	5	24	4
A369S	78	16	68	54		41	17	53	10
E370A	117	16	53	40		101	46	68	27
P371A	52	27	43	17		72	6	70	0
P372A	57	40	73	33		54	4	56	10
F373A	88	28	94	0		83	35	112	39
G374A	49	16	66	48		42	5	69	23
D375A	130	28	94	52		125	1	125	46
S376A	55	14	69	29		48	13	75	9
Y377A	113	12	84	2		74	29	105	10
I378A	31	22	95	163		42	22	32	10
I379A	66	34	62	24		68	25	82	10
I380A	2	1	0	4		-5	8	7	3

G381A	2	2	32	65		3	6	4	0
V382A	102	12	157	55		107	33	90	13
E383A	106	7	61	32		82	28	96	20
P384A	52	29	45	48		48	0	43	14
G385A	128	6	78	45		72	27	88	1
Q386A	127	6	89	13		101	39	99	36
L387A	35	2	18	14		20	12	44	7
K388A	78	39	92	0		105	40	99	40
L389A	42	10	23	15		31	14	34	6
N390A	111	75	94	16		114	69	106	27
W391A	26	16	42	71		22	18	37	14
F392A	104	10	75	27		72	2	75	28
K393A	86	11	67	23		28	3	54	7
K394A	124	5	78	31		75	58	98	33
G395A	109	56	129	50		87	42	79	7
S396A	119	36	86	41		113	1	106	8
S397A	131	37	51	2		76	9	108	40
I398A	108	15	85	62		107	1	114	28
G399A	120	16	97	53		118	81	91	43
Q400A	139	4	105	79		82	19	95	5
M401A	130	7	122	83		88	40	118	25
F402A	111	40	119	65		155	25	97	9
E403A	100	29	79	14		95	32	102	30
T404A	101	24	81	16		139	6	107	34
T405A	103	61	79	1		116	96	111	24
M406A	113	28	96	21		99	8	96	44
R407A	117	6	103	19		58	37	77	1
G408A	115	22	88	24		86	2	115	21
A409S	123	12	59	33		124	37	102	20
K410A	97	12	62	71		110	4	106	15
R411A	105	19	143	65		63	32	105	39
M412A	109	28	129	61		99	38	98	41
A413S	104	15	133	66		84	15	110	6
I414A	136	33	130	17		105	3	92	34
L415A	101	13	143	97		106	37	107	38
G416A	108	34	156	143		121	38	88	4
D417A	90	5	84	10		112	21	117	9
T418A	102	45	86	6		82	6	103	18
A419S	113	15	103	13		84	3	116	30
W420A	111	37	86	41		71	3	110	8
D421A	123	20	91	21		105	4	114	27
F422A	107	7	87	8		111	24	88	18
G423A	118	54	102	59		81	26	120	28
S424A	141	95	97	37		73	34	109	5
L425A	112	60	113	52		76	6	119	23
G426A	120	69	111	24		74	46	118	18
G427A	137	69	115	50		65	49	103	5
V428A	116	54	86	7		112	0	87	2

F429A	123	25	114	27		98	8	108	27
T430A	118	62	91	7		78	10	89	11
S431A	113	9	107	33		120	59	92	26
I432A	126	7	79	0		119	23	95	13
G433A	108	9	93	33		113	32	96	16
K434A	134	42	84	8		115	8	95	27
A435S	117	47	86	1		78	6	98	4
L436A	122	55	123	28		135	12	119	15
H437A	138	44	102	3		63	39	107	15
Q438A	133	11	138	103		92	49	106	33
V439A	96	0	92	4		82	7	106	34
F440A	116	44	107	50		78	8	112	6
G441A	141	71	84	27		77	8	123	15
A442S	114	35	109	37		57	21	96	24
I443A	110	15	99	7		114	24	105	11
Y444A	109	4	97	39		82	7	88	7
G445A	103	10	163	59		52	32	92	7
A446S	134	8	91	8		104	50	94	20
A447S	128	19	87	11		76	19	105	27
F448A	113	60	125	62		85	31	108	9
S449A	140	84	89	24		84	15	110	35
G450A	82	21	80	14		92	25	95	29
V451A	125	95	97	17		82	28	111	40
S452A	90	14	94	4		67	26	99	25
W453A	140	38	91	25		136	22	113	17
T454A	93	41	65			99	26	100	2
M455A	117	19	107	31		109	15	109	34
K456A	112	33	83	48		95	66	97	20
I457A	112	17	75	25		128	1	106	15
L458A	90	29	82	24		106	2	114	44
I459A	109	5	135	72		91	15	111	3
G460A	105	28	70	2		100	20	98	13
V461A	104	44	146	92		112	37	116	37
I462A	151	74	84	19		83	22	99	1
I463A	129	64	67	17		129	24	109	28
T464A	101	28	77	13		154	58	98	6
W465A	92	6	79	3		80	11	119	24
I466A	101	40	89	28		91	51	91	7
G467A	117	3	68	32		142	8	82	16
M468A	84	14	93	59		76	35	99	16
N469A	104	2	63			91	19	90	19
S470A	69	58	141	79		81	42	89	27
R471A	83	17	90	2		91	57	110	0
S472A	83	8	97	14		99	9	120	22
T473A	118	13	111	26		132	22	115	39
S474A	94	2	74	18		77	5	112	38
L475A	143	81	77	20		76	5	103	23
S476A	113	15	141	79		78	16	106	41

V477A	113	23	74	19		93	3	116	37
T478A	148	14	69	29		90	3	115	11
L479A	155	7	53	6		120	4	112	19
V480A	126	24	82	27		108	76	92	14
L481A	139	38	103	73		94	15	88	4
V482A	134	33	121	85		88	4	100	2
G483A	88	29	99	5		96	34	96	30
I484A	87	66	87	18		114	46	111	21
V485A	134	12	67	33		95	60	114	28
T486A	111	32	98	26		115	9	104	36
L487A	140	26	86	11		75	3	103	40
Y488A	146	64	80	22		91	67	109	26
L489A	111	30	119	49		74	23	92	3
G490A	125	68	100	26		70	9	107	22
V491A	106	43	62	2		79	17	112	15
M492A	106	55	74	54		100	38	113	24
V493A	130	57	108	91		92	3	91	9
Q494A	97	54	116	59		87	15	97	11
A495S	93	38	95	56		145	19	98	22

Table S2. Summary of Ig sequences, clonal families and their corresponding mean SHM in unstimulated PBMCs vs. stimulated PBMCs from DENV-infected patient 013.

	Unstimulated PBMCs	Stimulated PBMCs
HC all unique reads	162928	1245789
HC sequences with UMI ≥ 2	18588	146287
HC clonal families	11596	11407
IgM sequences	15318	4684
SHM, IgM sequences	0.6%	2.7%
IgG sequences	2156	129636
SHM, IgG sequences	6.7%	7.0%
IgA sequences	1114	11967
SHM, IgA sequences	7.0%	6.2%
Unique clonal family threshold	17.8%	21.4%
IgM clonal families	9794	2260
SHM, IgM clonal families	0.6%	1.9%
IgG clonal families	1243	5657
SHM, IgG clonal families	6.0%	5.6%
IgA clonal families	559	3490
SHM, IgA clonal families	6.9%	6.3%

Table S3. Sequences from unstimulated PBMCs or stimulated PBMCs related to the clonal families of single cell plasmablasts with reactivity to dengue virus isolated from patient 013.

Clonal family (mAbs)	Germline	Isotype	Reads for all clonotypes	
			Unstimulated PBMCs	Stimulated PBMCs
CF10	IGHV3-30-3	total	143	216292
(C1, A7, I11, L9, P2, G5)		IgM	8	427
		IgG	112	199151
		IgA	23	16714
CF5	IGHV1-69	total	422	141308
(C4, J2, N2)		IgM	9	91
		IgG	413	140117
		IgA	0	1100
CF13	IGHV4-34	total	32	82814
(N8, F4)		IgM	0	195
		IgG	32	76605
		IgA	0	6014
CF7	IGHV1-69	total	579	43179
(J8, J9)		IgM	10	98
		IgG	568	42315
		IgA	1	764
CF9	IGHV1-69	total	673	35793
(K11, L3, M4, M11, O4)		IgM	12	103
		IgG	656	34444
		IgA	5	1246
CF8	IGHV1-69	total	10	7349
(J3, 403_P4)		IgM	0	16

		IgG	10	7001
		IgA	0	332
CF3 (405_P4, I13)	IGHV1-18	total	10	2993
		IgM	1	6
		IgG	9	2899
		IgA	0	88
CF1 (B10, M1, D8)	IGHV4-39	total	4	1087
		IgM	1	11
		IgG	3	1049
		IgA	0	27
CF2 (H3, M6)	IGHV1-69	total	0	1087
		IgM	0	7
		IgG	0	1066
		IgA	0	14
CF11 (E9, I8)	IGHV3-30-3	total	0	19
		IgM	0	0
		IgG	0	19
		IgA	0	0

Figure S1

Patient ID	Clonal family ID	mAb name	VH			VL			Crude [IgG]	Fold change in binding		% Neutralization					
			Gene	% nt mutation	CDR3 aa length	Gene	% nt mutation	CDR3 aa length	(ug/mL)	DENV2 rE	DENV2 RVP	DENV1	DENV2	DENV3	DENV4	ZIKV	WNV
020	**CF1**	**B10**	**4-39**	**2.68**	**10**	**1-9**	**2.47**	**9**	**3.21**	**6**	**12**	**65**	**43**	**64**	**69**	**38**	**11**
013		**M1**	**4-39**	**10.77**	**10**	**1-9**	**1.06**	**9**	**4.77**	**4**	**13**	**73**	**77**	**65**	**84**	**33**	**47**
020		D8	4-39	5.30	10	1-9	2.13	9	1.77	2	15	48	41	55	42	28	44
013	CF2	M6	1-69	2.72	15	1-40	4.73	11	4.88	2	1	-6	10	36	53	27	36
013		H3	1-69	5.44	15	1-5	3.48	10	1.26	34	7	41	72	64	84	0	47
013	CF3	P4(405)	1-18	7.53	16	2-14	1.68	10	<0.0005	n/a	n/a	n/a	n/a	n/a	n/a	n/a	n/a
013		I13	1-18	7.53	16	2-14	3.37	10	<0.0005	n/a	n/a	n/a	n/a	n/a	n/a	n/a	n/a
020	**CF4**	**I7**	**1-3**	**5.42**	**16**	**1-39**	**7.04**	**9**	**1.65**	**34**	**14**	**41**	**67**	**57**	**49**	**13**	**76**
013	**CF5**	**C4**	**1-69**	**10.17**	**17**	**1-5**	**2.12**	**8**	**2.47**	**1**	**1**	**96**	**74**	**96**	**65**	**22**	**46**
013		J2	1-69	10.51	17	1-5	2.47	8	<0.0005	n/a	n/a	n/a	n/a	n/a	n/a	n/a	n/a
013		N2	1-69	8.81	17	1-5	2.12	8	1.97	1	1	98	-10	65	69	3	39
020	**CF6**	**L8**	**1-69**	**4.07**	**13**	**1-40**	**0.67**	**12**	**3.93**	**9**	**7**	**68**	**81**	**78**	**92**	**28**	**45**
020		H1	1-69	4.41	13	1-40	0.67	12	<0.0005	n/a	n/a	n/a	n/a	n/a	n/a	n/a	n/a
013	**CF7**	J8	1-69	9.86	16	3-11	1.39	12	<0.0005	n/a	n/a	n/a	n/a	n/a	n/a	n/a	n/a
013		**J9**	**1-69**	**10.44**	**16**	**3-11**	**3.83**	**12**	**4.04**	**1**	**5**	**100**	**100**	**100**	**100**	**20**	**29**
013	CF8	J3	1-69	9.22	17	2-14	7.22	12	0.95	1	2	97	59	74	40	6	30
013		P4(403)	1-69	7.51	17	2-14	3.48	12	2.35	1	1	100	44	78	43	5	25
013	CF9	M11	1-69	8.45	20	3-15	3.48	9	4.04	1	2	100	39	59	56	25	49
013		M4	1-69	6.76	20	3-15	2.44	9	2.54	1	1	100	1	39	40	5	33
013		L3	1-69	5.07	20	3-15	2.44	9	2.40	1	2	100	18	53	53	22	45
013		K11	1-69	6.08	20	3-15	2.79	9	3.97	1	1	100	-17	47	44	14	33
013		O4	1-69	7.43	20	3-15	2.44	9	1.74	1	1	100	0	40	58	5	34
013	CF10	I11	3-30-3	3.08	14	3-15	1.77	8	1.61	2	3	84	10	31	57	14	22
013		C1	3-30-3	4.11	14	3-15	3.92	8	<0.0005	n/a	n/a	n/a	n/a	n/a	n/a	n/a	n/a
013		G5	3-30-3	4.80	14	3-15	1.43	8	nc	n/a	n/a	n/a	n/a	n/a	n/a	n/a	n/a
013		P2	3-30-3	5.14	14	3-15	3.90	8	4.13	1	1	96	16	34	49	7	28
013		A7	3-30-3	10.27	14	3-15	4.26	8	2.16	1	2	97	30	20	55	14	32
013		L9	3-30-3	5.78	14	3-15	4.26	8	1.92	39	2	-16	0	52	78	19	35
013	CF11	E9	3-30-3	8.11	23	1-40	3.43	10	<0.0005	n/a	n/a	n/a	n/a	n/a	n/a	n/a	n/a
013		I8	3-30-3	8.78	23	1-40	4.45	10	nc	n/a	n/a	n/a	n/a	n/a	n/a	n/a	n/a
020	CF12	E1	3-7	2.71	17	8-61	2.03	10	<0.0005	n/a	n/a	n/a	n/a	n/a	n/a	n/a	n/a
020		F10	3-7	4.41	17	8-61	2.70	10	3.96	2	3	-28	-8	40	63	6	15
013	CF13	N8	4-34	7.85	18	2-14	6.49	12	2.55	1	1	99	0	34	61	4	11
013		F4	4-34	5.12	18	2-14	3.05	12	1.41	1	1	100	1	48	58	6	20
020	CF14	K2	4-39	2.34	15	1-5	1.76	8	2.09	1	1	-32	24	44	54	26	39
020		A5	4-39	1.67	15	1-5	1.41	8	3.63	1	1	-5	23	53	75	20	37
013	CF15	P10	4-59	6.21	23	1-39	2.11	8	0.72	1	11	25	68	66	74	27	20
013		L2	4-59	7.29	23	1-39	6.43	8	4.66	1	14	10	61	60	61	25	9
3H5-1	DENV2-specific mAb		n/a	n/a	n/a	n/a	n/a	n/a	n/a	44	10	nd	nd	nd	nd	nd	nd
EDE2 B7	DENV cross-reactive mAb		3-74	6.94	26	2-23	4.51	10	n/a	1	3	nd	nd	nd	nd	nd	nd
EDE1 C10	DENV cross-reactive mAb		1-3	2.78	21	2-14	3.82	10	n/a	nd	nd	100	99	92	100	99	-99
CR4354	WNV-specific mAb		n/a	n/a	n/a	n/a	n/a	n/a	n/a	nd	nd	-127	-57	-149	-139	-48	93

Fold change in binding
≥11
5-10
2-4
1

% Neutralization
90-100
75-89
51-74
≤50

Figure S2

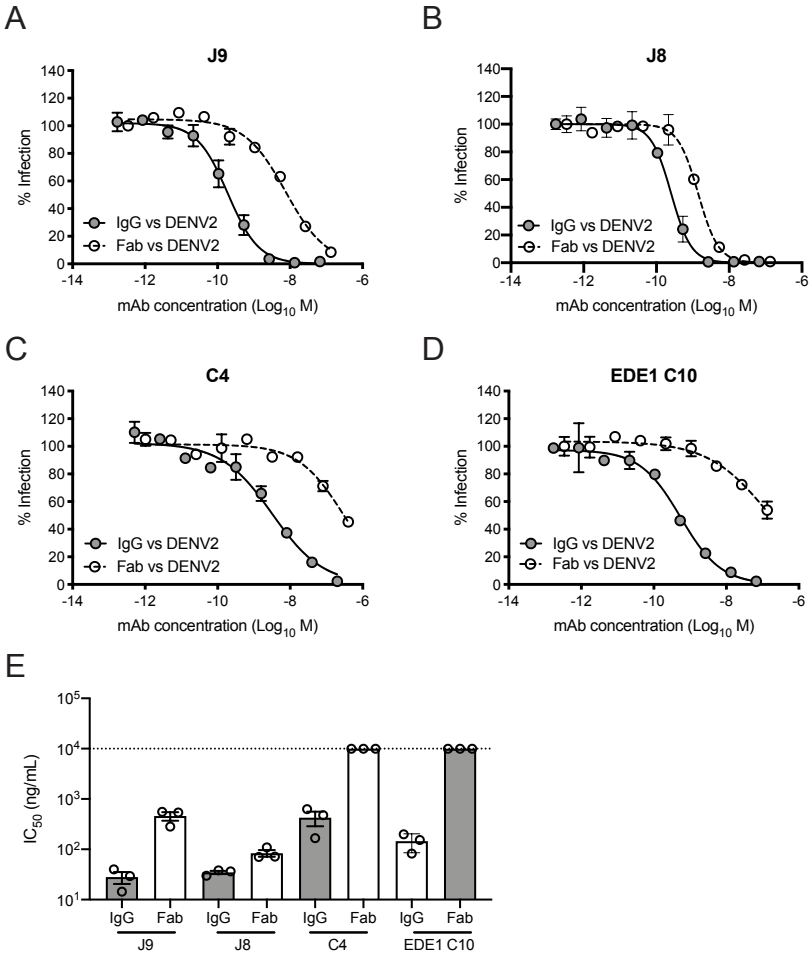

Figure S3

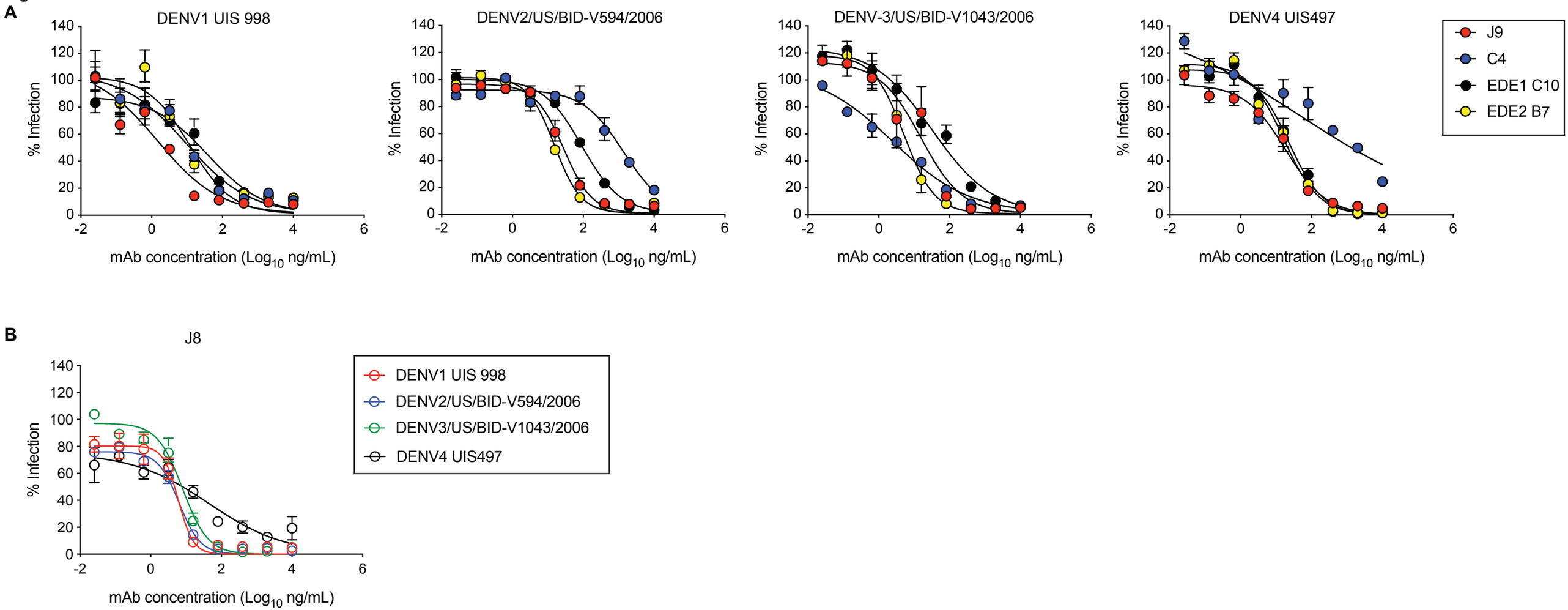
A
DENV1 UIS 998
DENV2/US/BID-V594/2006
DENV-3/US/BID-V1043/2006
DENV4 UIS497
% Infection
mAb concentration (Log10 ng/mL)
J9
C4
EDE1 C10
EDE2 B7
B
J8
DENV1 UIS 998
DENV2/US/BID-V594/2006
DENV3/US/BID-V1043/2006
DENV4 UIS497

Figure S4

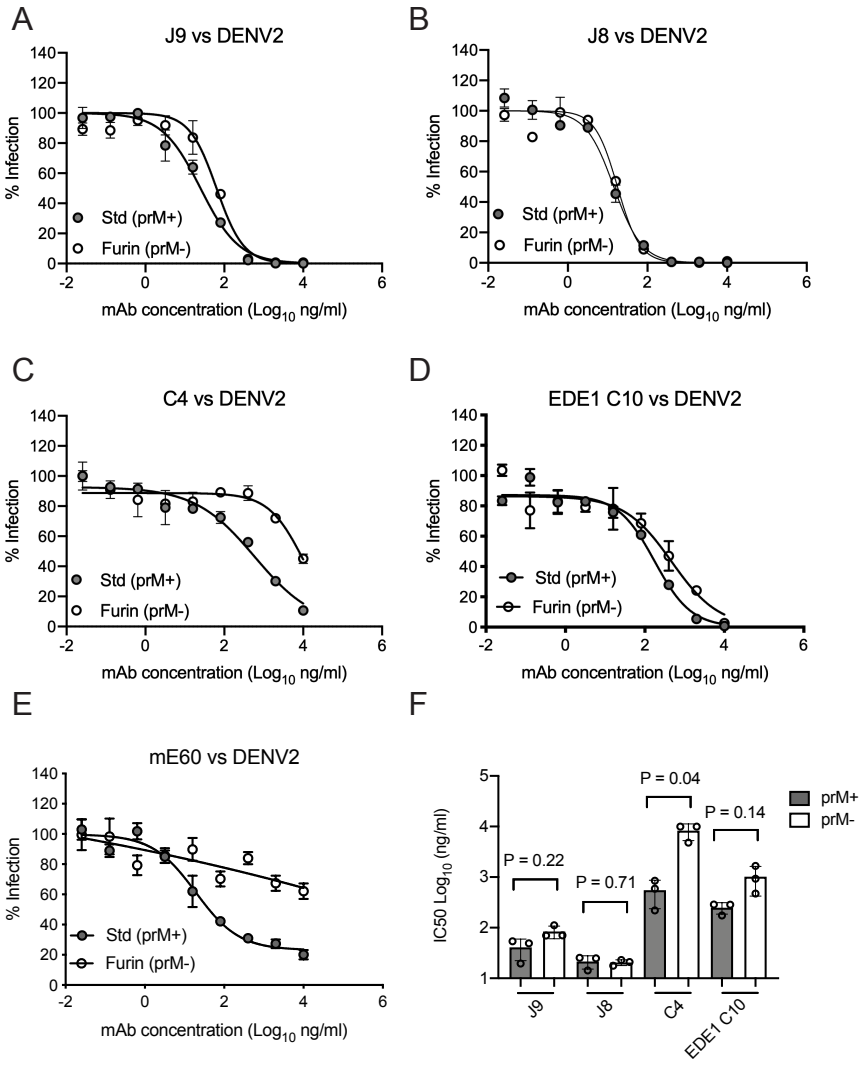

Figure S5

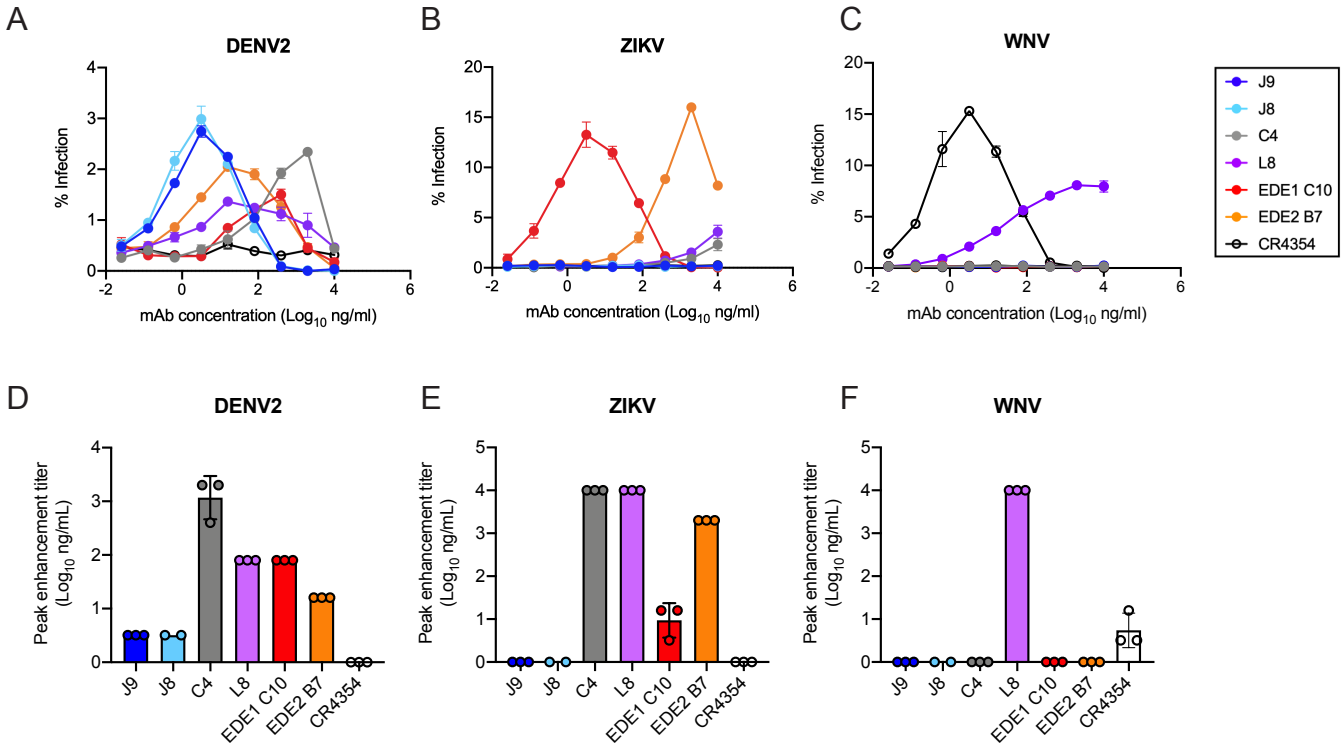

Figure S6

A

```
DENV1_WP_AAN06983.1          MRCVGIGNRDFVEGLSGATWVDVVLEHGSCVTTMAKDKPTLDIELLKTEVTNPAVLRKLC   60
DENV2_16681_NP_739583.2      MRCIGMSNRDFVEGVSGGSWVDIVLEHGSCVTTMAKNKPTLDFELIKTEAKQPATLRKYC   60
DENV3_CH53489_AAB69126.2     MRCVGVGNRDFVEGLSGATWVDVVLEHGGCVTTMAKNKPTLDIELQKTEATQLATLRKLC   60
DENV4_TVP360_ANK35835.1      MRCVGVGNRDFVEGVSGGAWVDLVLEHGGCVTTMAQGKPTLDFELTKTTAKEVALLRTYC   60
ZIKV_HPF2013_AHZ13508.1      IRCIGVSNRDFVEGMSGGTWVDVVLEHGGCVTVMAQDKPTVDIELVTTTVSNMAEVRSYC   60
WNVI_NY99_ADD23565.1         FNCLGMSNRDFLEGVSGATWVDLVLEGDSCVTIMSKDKPTIDVKMMNMEAANLAEVRSYC   60
JEV_SA14_AAA21436.1          FNCLGMGNRDFIEGASGATWVDLVLEGDSCLTIMANDKPTLDVRMINIEASQLAEVRSYC   60
YFV_Asibi_AHB63685.1         AHCIGITDRDFIEGVHGGTWVSATLEQDKCVTVMAPDKPSLDISLETVAIDGPAEARKVC   60

DENV1_WP_AAN06983.1          IEAKISNTTTDSRCPTQGEATLVEEQDTNFVCRRTFVDRGWGNGCGLFGKGSLITCAKFK  120
DENV2_16681_NP_739583.2      IEAKLTNTTTESRCPTQGEPSLNEEQDKRFVCKHSMVDRGWGNGCGLFGKGGIVTCAMFR  120
DENV3_CH53489_AAB69126.2     IEGKITNITTDSRCPTQGEAILPEEQDQNYVCKHTYVDRGWGNGCGLFGKGSLVTCAKFQ  120
DENV4_TVP360_ANK35835.1      IEASISNITTATRCPTQGEPYLKEEQDQQYICRRDVVDRGWGNGCGLFGKGGVVTCAKFS  120
ZIKV_HPF2013_AHZ13508.1      YEASISDMASDSRCPTQGEAYLDKQSDTQYVCKRTLVDRGWGNGCGLFGKGSLVTCAKFA  120
WNVI_NY99_ADD23565.1         YLATVSDLSTKAACPTMGEAHNDKRADPAFVCRQGVVDRGWGNGCGLFGKGSIDTCAKFA  120
JEV_SA14_AAA21436.1          YHASVTDISTVARCPTTGEAHNEKRADSSYVCKQGFTDRGWGNGCGLFGKGSIDTCAKFS  120
YFV_Asibi_AHB63685.1         YNAVLTHVKINDKCPSTGEAHLAEENEGDNACKRTYSDRGWGNGCGLFGKGSIVACAKFT  120

DENV1_WP_AAN06983.1          CVTKLEGKIVQYENLKYSVIVTVHTGDQ---H-----QVGNETTEHGTTATITPQAPTSE  172
DENV2_16681_NP_739583.2      CKKNMEGKVVQPENLEYTIVITPHSGEE---H-----AVGNDTGKHGKEIKITPQSSITE  172
DENV3_CH53489_AAB69126.2     CLESIEGKVVQHENLKYTVIITVHTGDQ---H-----QVGNET--QGVTAEITPQASTVE  170
DENV4_TVP360_ANK35835.1      CSGKITGNLVQIENLEYTVVVTVHNGDT---H-----AVGNDTSNHGVTAMITPRSPSVE  172
ZIKV_HPF2013_AHZ13508.1      CSKKMTGKSIQPENLEYRIMLSVHGSQH---SGMIVNDTGHETDENRAKVEITPNSPRAE  177
WNVI_NY99_ADD23565.1         CSTKAIGRTILKENIKYEVAIFVHGPTTVESHGNYSTQVGA---TQAGRFSITPAAPSYT  177
JEV_SA14_AAA21436.1          CTSKAIGRTIQPENIKYEVGIFVHGTTTSENHGNYSAQVGA---SQAAKFTVTPNAPSIT  177
YFV_Asibi_AHB63685.1         CAKSMSLFEVDQTKIQYVIRAQLHVGAKQENW---N--------TDIKTLKFDALSGSQE  169

DENV1_WP_AAN06983.1          IQLTDYGALTLDCSPRTGLDFNEMVLLTMEKKSWLVHKQWFLDLPLPWTSGASTSQETWN  232
DENV2_16681_NP_739583.2      AELTGYGTVTMECSPRTGLDFNEMVLLQMENKAWLVHRQWFLDLPLPWLPGADTQGSNWI  232
DENV3_CH53489_AAB69126.2     AILPEYGTLGLECSPRTGLDFNEMILLTMKNKAWMVHRQWFFDLPLPWTSGATTETPTWN  230
DENV4_TVP360_ANK35835.1      VKLPDYGELTLDCEPRSGIDFNEMILMKMKKKTWLVHKQWFLDLPLPWTAGADTSEVHWN  232
ZIKV_HPF2013_AHZ13508.1      ATLGGFGSLGLDCEPRTGLDFSDLYYLTMNNKHWLVHKEWFHDIPLPWHAGADTGTPHWN  237
WNVI_NY99_ADD23565.1         LKLGEYGEVTVDCEPRSGIDTNAYYVMTVGTKTFLVHREWFMDLNLPWSSAG---STVWR  234
JEV_SA14_AAA21436.1          LKLGDYGEVTLDCEPRSGLNTEAFYVMTVGSKSFLVHREWFHDLALPWTSPS---STAWR  234
YFV_Asibi_AHB63685.1         AEFTGYGKATLECQVQTAVDFGNSYIAEMEKESWIVDRQWAQDLTLPWQSGS---GGVWR  226

DENV1_WP_AAN06983.1          RQDLLVTFKTAHAKKQEVVVLGSQEGAMHTALTGATEIQTSGT----TTIFAGHLKCRLK  288
DENV2_16681_NP_739583.2      QKETLVTFKNPHAKKQDVVVLGSQEGAMHTALTGATEIQMSSG----NLLFTGHLKCRLR  288
DENV3_CH53489_AAB69126.2     RKELLVTFKNAHAKKQEVVVLGSQEGAMHTALTGATEIQNSGG----TSIFAGHLKCRLK  286
DENV4_TVP360_ANK35835.1      YKERMVTFKVPHAKRQDVTVLGSQEGAMHSALAGATEVDSGDG----NHMFAGHLKCKVR  288
ZIKV_HPF2013_AHZ13508.1      NKEALVEFRDAHAKRQTVVVLGSQEGAVHTALAGALEAEMDGAK---GRLSSGHLKCRLK  294
WNVI_NY99_ADD23565.1         NRETLMEFEEPHATKQSVIALGSQEGALHQALAGAIPVEFSSNT---VKLTSGHLKCRVK  291
JEV_SA14_AAA21436.1          NRELLMEFEEAHATKQSVVALGSQEGGLHQALAGAIVVEYSS-S---VKLTSGHLKCRLK  290
YFV_Asibi_AHB63685.1         EMHHLVEFEPPHAATIRVLALGNQEGSLKTALTGAMRVTKDTNDNNLYKLHGGHVSCRVK  286

DENV1_WP_AAN06983.1          MDKLTLKGMSYVMCTGSFKLEKEVAETQHGTVLVQVKYEGTDAPCKIPFSSQ-DEKGVTQ  347
DENV2_16681_NP_739583.2      MDKLQLKGMSYSMCTGKFKVVKEIAETQHGTIVIRVQYEGDGSPCKIPFEIM-DLEKRHV  347
DENV3_CH53489_AAB69126.2     MDKLELKGMSYAMCLNTFVLKKEVSETQHGTILIKVEYKGEDAPCKIPFSTE-DGQGKAH  345
DENV4_TVP360_ANK35835.1      MEKLRIKGMSYTMCSGKFSIDKEMAETQHGTTVVKVKYEGAGAPCKVPIEIR-DVNKEKV  347
ZIKV_HPF2013_AHZ13508.1      MDKLRLKGVSYSLCTAAFTFTKIPAETLHGTVTVEVQYAGTDGPCKVPAQIAVDMQTLTP  354
WNVI_NY99_ADD23565.1         MEKLQLKGTTYGVCSKAFKFLGTPADTGHGTVVLELQYTGTDGPCKVPISSVASLNDLTP  351
JEV_SA14_AAA21436.1          MDKLALKGTTYGMCTEKFSFAKNPADTGHGTVVIELSYSGSDGPCKIPIVSVASLNDMTP  350
YFV_Asibi_AHB63685.1         LSALTLKGTSYKMCTDKMSFVKNPTDTGHGTVVMQVKVP-KGAPCKIPVIVADDLTAAIN  345

DENV1_WP_AAN06983.1          NGRLITANPIVTDKE--KPVNIEAEPPFGESYIVVGAGEKALKLSWFKKG     395
DENV2_16681_NP_739583.2      LGRLITVNPIVTEKD--SPVNIEAEPPFGDSYIIIGVEPGQLKLNWFKKG     395
DENV3_CH53489_AAB69126.2     NGRLITANPVVTKKE--EPVNIEAEPPFGESNIVIGIGDKALKINWYKKG     393
DENV4_TVP360_ANK35835.1      VGRIISSTPLAENTN--SVTNIELEPPFGDSYIVIGVGNSALTLHWFRKG     395
ZIKV_HPF2013_AHZ13508.1      VGRLITANPVITESTENSKMMLELDPPFGDSYIVIGVGEKKITHHWHRSG     404
WNVI_NY99_ADD23565.1         VGRLVTVNPFVSVATANAKVLIELEPPFGDSYIVVGRGEQQINHHWHKSG     401
JEV_SA14_AAA21436.1          VGRLVTVNPFVATSSANSKVLVEMEPPFGDSYIVVGRGDKQINHHWHKAG     400
YFV_Asibi_AHB63685.1         KGILVTVNPIASTND--DEVLIEVNPPFGDSYIIVGTGDSRLTYQWHKEG     393
```

B

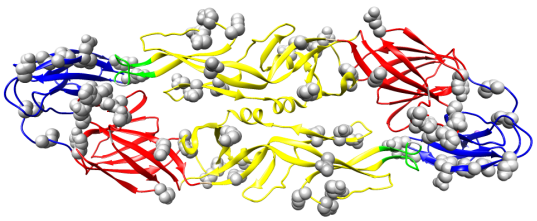

C

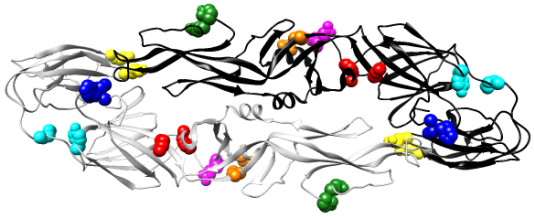

Figure S7

A

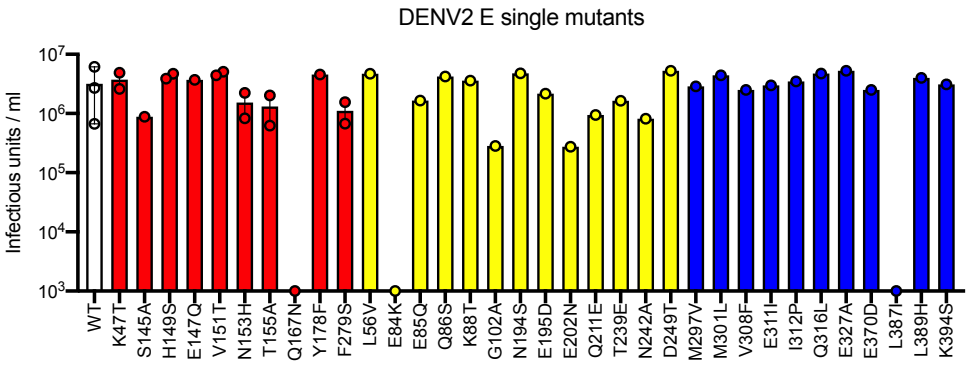

B

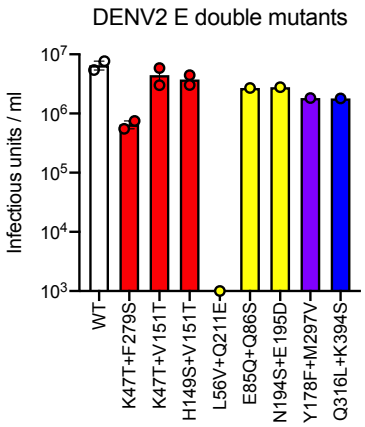

Figure S8

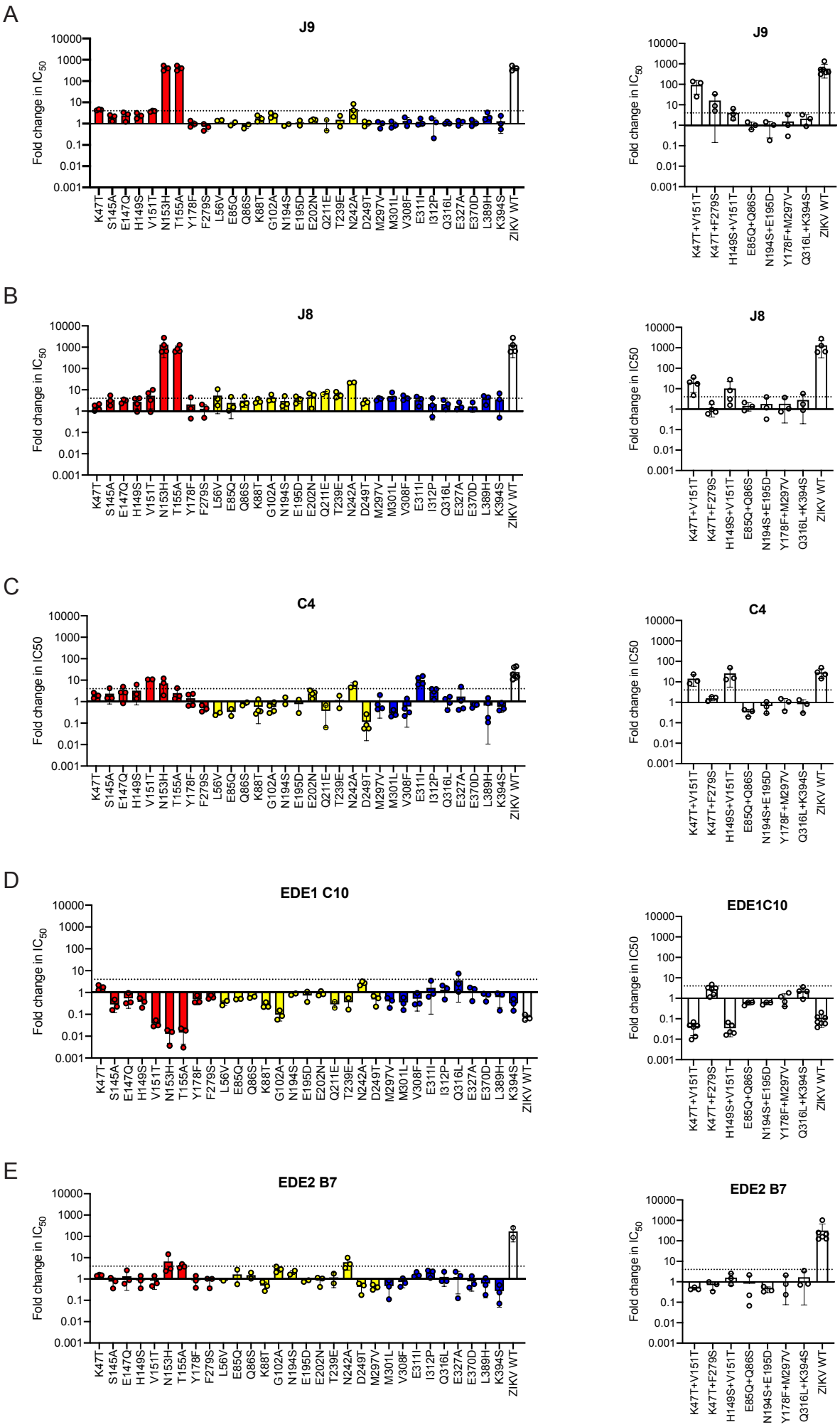

Figure S9

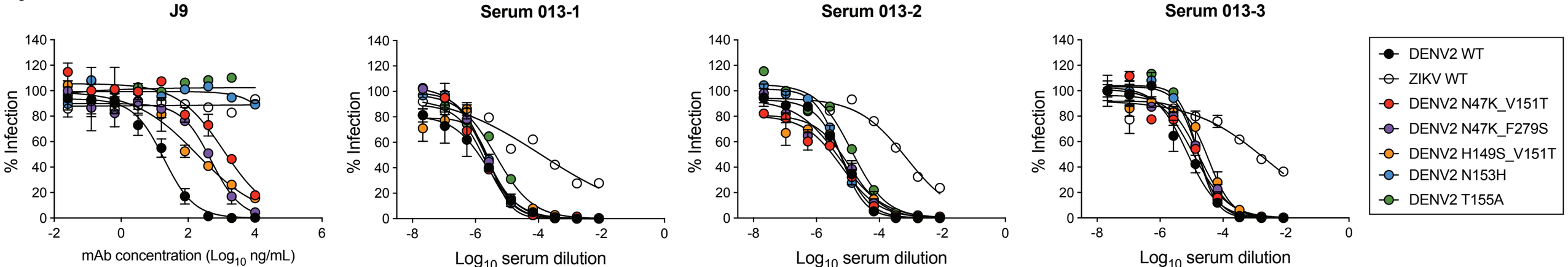
J9
Serum 013-1
Serum 013-2
Serum 013-3
% Infection
mAb concentration (Log10 ng/mL)
Log10 serum dilution
DENV2 WT
ZIKV WT
DENV2 N47K_V151T
DENV2 N47K_F279S
DENV2 H149S_V151T
DENV2 N153H
DENV2 T155A

Figure S10

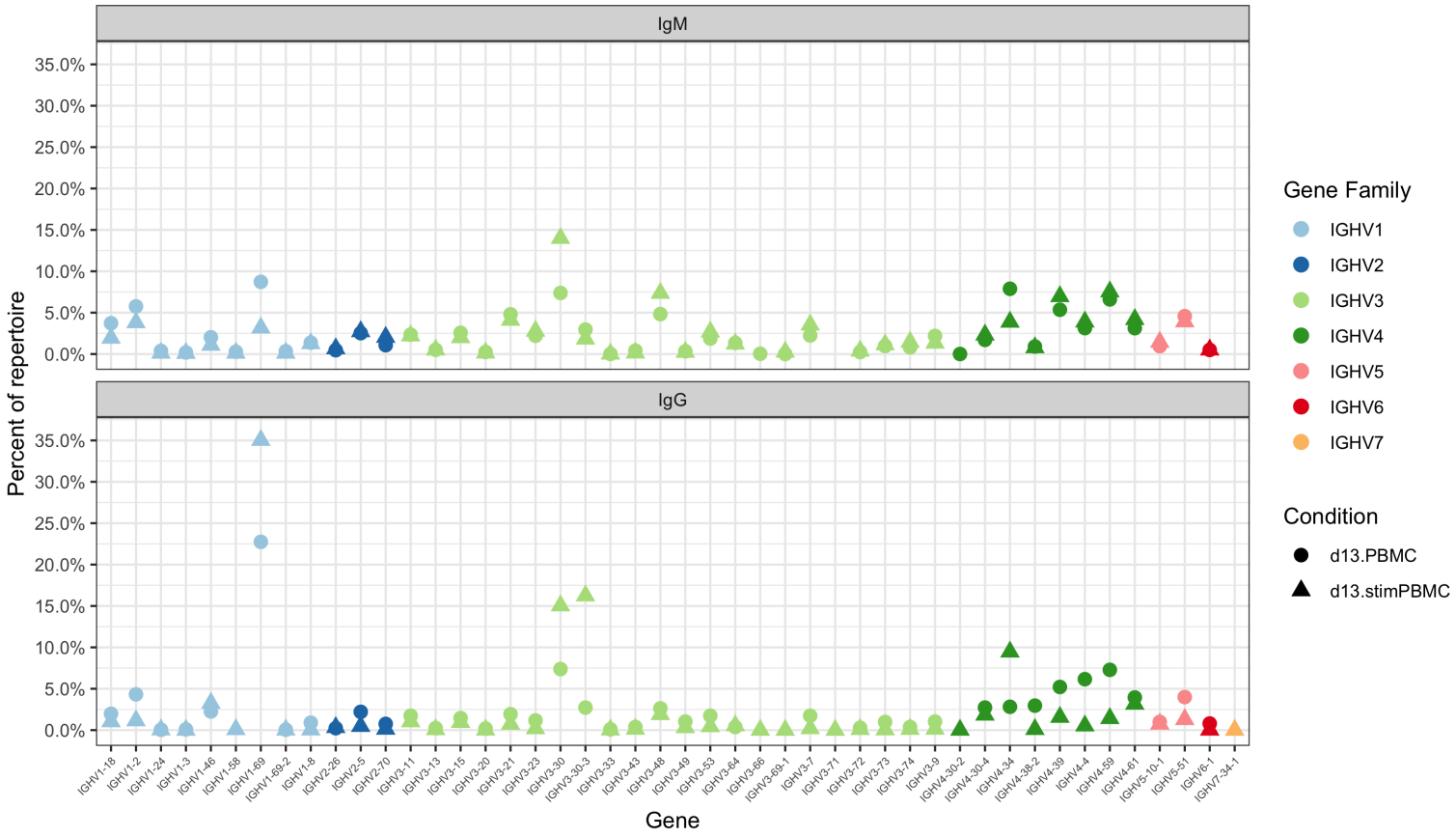

Figure S11